A Hybrid Estimator for Active/Reactive Power Control of Single-Phase Distributed Generation Systems With Energy Storage

Majid Pahlevani, *Senior Member, IEEE*, Suzan Eren, *Member, IEEE*, Josep M. Guerrero, *Fellow, IEEE*, and Praveen Jain, *Fellow, IEEE*

***Abstract*—This paper presents a new active/reactive power closed-loop control system for a hybrid renewable energy generation system used for single-phase residential/commercial applications. The proposed active/reactive control method includes a hybrid estimator, which is able to quickly and accurately estimate the active/reactive power values. The proposed control system enables the hybrid renewable energy generation system to be able to perform real-time grid interconnection services such as active voltage regulation, active power control, and fault ride-through. Simulation and experimental results demonstrate the superior performance of the proposed closed-loop control system.**

***Index Terms*—Ac/dc converter, adaptive estimator, bidirectional converter, dc/dc converter, double-frequency ripple, grid-connected converter, renewable energy, state observer.**

I. Introduction

HARVESTING energy from renewable sources such as solar and wind energy has recently gained a large momentum due mostly to environmental reasons. Nowadays, people consider renewable energy sources to be a viable mainstream source of power generation. In the ideal case, a residential house should be self-sustainable and even support the utility grid when needed. The main difficulty in realizing this scheme is the intermittent nature of renewable energy sources [1]–[3]. Therefore, reliability is the main concern for harvesting renewable energy in the future. Energy storage systems offer a great solution to complement the intermittent nature of renewable energy systems [4]–[6]. In particular, energy storage in the form of batteries in electric vehicles (EVs) can effectively support the integration of the intermittent renewable energy sources into distributed generations (DGs) [7]–[10]. With the exponential growth of EVs, the batteries in EVs can offer substantial energy storage capacity for DGs. Besides energy storage, EVs can offer reactive power compensation (*VAR* compensation), load balancing, current harmonic filtering and several other ancillary services [11], [12]. Considering the aforementioned capabilities, EVs and energy storage units will be an inevitable part of smart grids [13]–[18]. Fig. 1 shows a typical arrangement of a hybrid renewable energy generation system (HREGS). According to this figure, a wind energy conversion system (WECS), a solar inverter and an energy storage unit are included in the HREGS. These three components perform intelligent energy management. Only during days is the solar inverter producing power, whereas the wind power generation is more pronounced during nights. Using intelligent energy management, such as peak shaving or power shifting, the extra power can be stored in the energy storage unit and be released when it is required [19], [20].

From the aforementioned discussion, the importance of the energy storage unit is very evident in order to complement an intermittent HREGS. The focus of this paper is the active and reactive power control of the energy storage unit used in a residential scale HREGS. A single-phase bidirectional ac/dc converter is the key component of an energy storage unit. If an EV is used as the energy storage unit in this structure, the ac/dc converter is included in the on-board charger. The bidirectional ac/dc converter can effectively control the active and reactive power between the grid and the battery as well as performing other ancillary services. The control of the ac/dc converter is of great importance to the integration of the energy storage unit into the HREGS.

In single-phase systems, the real-time control of active/reactive power is challenging due to the presence of power ripple [21]–[24]. Conventionally, the active/reactive power control in ac/dc converters is performed either in a stationary reference frame or a synchronous reference frame (synchronous with the grid voltage). Real-time calculations of the active and reactive power for the feedback control system in a single-phase system requires low bandwidth filtering due to the double frequency power ripple. Herein lies the difficulty with the conventional control system. Thus, this paper presents a novel hybrid observer, which is able to eliminate the need for filtering the double frequency ripple in the instantaneous power signal, resulting in a fast response in the active/reactive power closed-loop control system.

In three-phase systems, calculating the active and reactive power is fairly simple. Conventionally, the Clarke transformation is used to convert the three-phase variables to a rotating vector in the stationary $\alpha\beta$-frame, then the Park transformation is used to convert the rotating vector to a stationary vector in the rotating dq-frame [25]. In single-phase systems, the same idea can be applied by generating an orthogonal signal

Manuscript received January 14, 2015; revised May 15, 2015; accepted July 1, 2015. Date of publication July 8, 2015; date of current version November 30, 2015. Recommended for publication by Associate Editor Y. Sozer.

M. Pahlevani, S. Eren, and P. Jain are with the Centre for Energy and Power Electronics Research, Queen's University, Kingston, ON K7L 3N6 Canada (e-mail: majidpahlevani@gmail.com; 2se1@queensu.ca; praveen.jain@queensu.ca).

J. M. Guerrero is with the Department of Energy Technology, Aalborg University, 9220 Aalborg East, Denmark (e-mail: joz@et.aau.dk).

Color versions of one or more of the figures in this paper are available online at http://ieeexplore.ieee.org.

Digital Object Identifier 10.1109/TPEL.2015.2453350

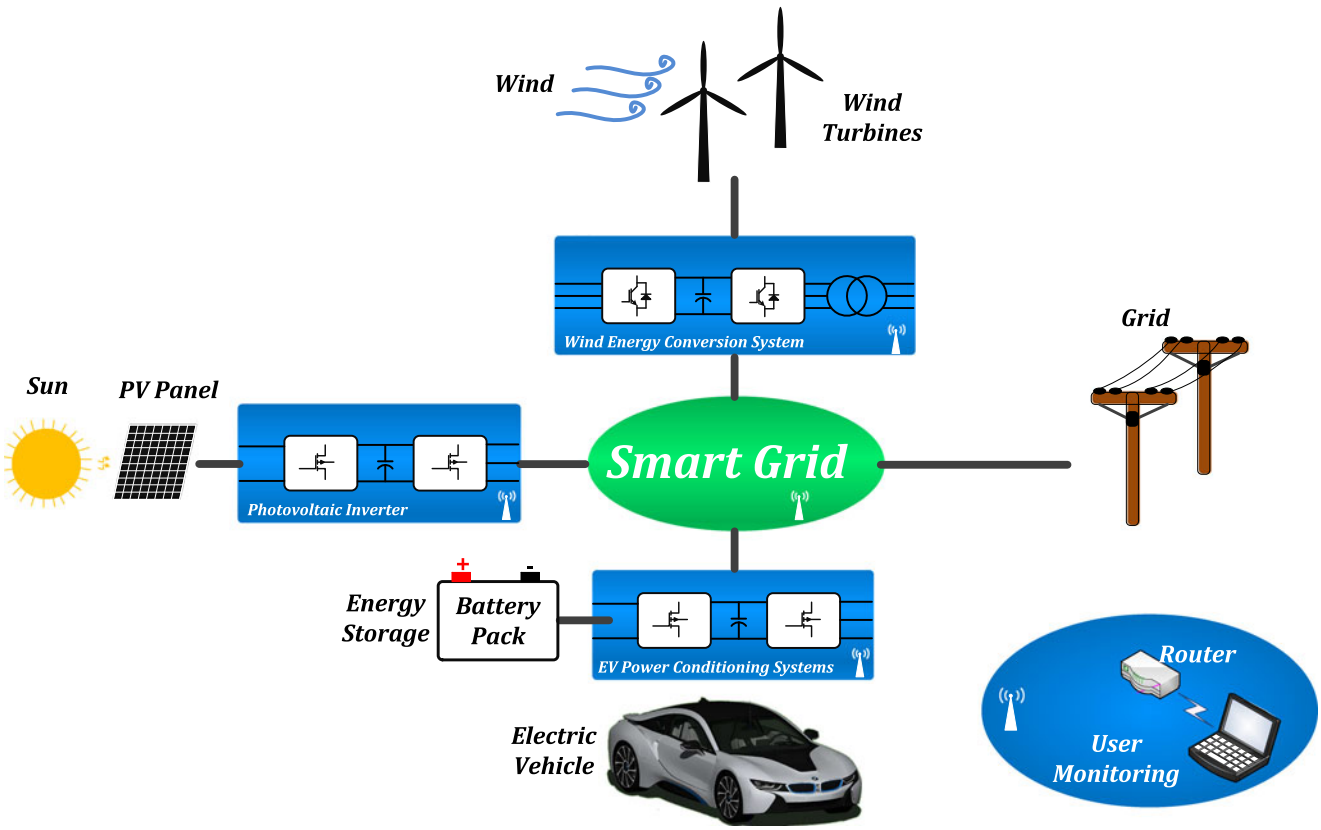

Fig. 1. HREGS for residential/commercial applications.

from the main signal, and then using the same concept to extract the active and reactive power in a single-phase system [26]–[31]. Although this technique can effectively extract the active and reactive power from the instantaneous power signal, the orthogonal signal generation can add complexity and delay to the active/reactive power calculations. Recently, the second-order generalized integrator (SOGI) has been used for grid synchronization [65]–[69]. This technique utilizes two integrators in order to generate orthogonal signals and use them to extract the phase/frequency information. This technique is a very good candidate for grid synchronization. The active and reactive power can also be estimated by using the orthogonal signal generator for the grid current as well as the grid voltage. Then, through having the orthogonal signals for the current and the voltage, the active and reactive power can be estimated. Although this technique provides a simple and practical solution for grid synchronization, it involves a rather complicated algorithm for measuring the active and reactive power due to the fact that the amplitudes and phases of both the voltage and current should be calculated. This method is also very susceptible to the harmonic content of the grid voltage and grid current. In order to mitigate the impact of harmonics, multiple modules should be implemented for different harmonics, which is called the multiple second order generalized integrator frequency-lock loop (MSOGI- FLL) [68]. The adaptive notch filter (ANF) is another grid synchronization method that can be used to extract the phase/frequency information [71]–[74]. The structure of the ANF, like the SOGI, also generates orthogonal signals. However, the frequency calculation using the orthogonal signals is performed differently. Similarly, the ANF can be used to estimate the active and reactive power. However, it has the same difficulties as the SOGI for active and reactive power estimation.

Another technique used to calculate the active and reactive power is the discrete Fourier transform (DFT). DFT can calculate the amplitude and angle of the voltage and current signals, and in turn, calculate the active and reactive power. However, the DFT requires at least one line cycle to precisely calculate the amplitude and phase of a signal. Thus, this method cannot be used to implement the real-time active/reactive power control required in future smart grid applications. In this paper, a hybrid estimator is proposed, which is able to rapidly estimate the active and reactive power generated/drawn by the ac/dc converter. Therefore, the proposed approach can be the solution for applications where real-time active power control and reactive power compensation is required. To the best of the authors knowledge, the proposed hybrid estimator is the only estimator with proven global asymptotic stability for this application. The specific structure of the hybrid estimator offers global asymptotic stability, which leads to a reliable and robust closed-loop control system for active and reactive power control.

This paper is organized as follows. A summary of intelligent energy management for grid-connected power converters is presented in Section II. The proposed hybrid estimator for active/reactive power control of the ac/dc converter is presented in

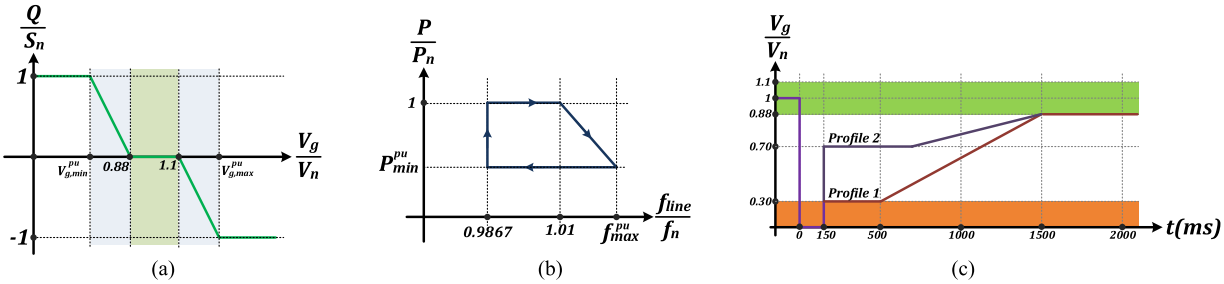

(a) (b) (c)

Fig. 2. Smart grid functionality.

Section III. Section IV presents the closed-loop control system of the ac/dc converter. Section V includes the stability analysis of the proposed hybrid estimator. A comparative study of the proposed hybrid estimator is presented in Section VI. The performance of the closed-loop control system is evaluated through computer simulations in Section VII. In Section VIII, the experimental results obtained from an ac/dc converter prototype are presented. Finally, Section IX is the conclusion.

II. Intelligent Energy Management for Grid-Connected Power Converters

In order to implement a reliable HREGS with intelligent energy management for residential applications, the power converters interfacing the utility grid must be able to perform several functions, such as active power control, reactive power compensation, active voltage regulation, and fault ride-through [32]–[34]. In this section, brief descriptions of these different functions are presented in order to elaborate on the emerging grid-connection requirements.

Currently, the regulatory standards for power converters interconnected with DGs (e.g., *UL1741*, and *IEEE 1547*) require the power conditioning system to be disconnected from the utility grid in case of abnormal conditions [35]–[37]. For instance, if the output voltage of the converter (grid voltage) is less than 88% or greater than 110% of the nominal voltage, the converter must be disconnected from the grid [35]. This requirement is imposed in order to save the equipment in fault/over voltage conditions. However, as DGs get more dominant, regulating the voltage to be in this range is very difficult. Therefore, the concept of having active voltage regulation provided by the renewable energy power conditioning system in the near future is becoming inevitable. By injecting reactive power, the active voltage regulation can be performed locally [38] in order to maintain the voltage level and avoid disconnection. Fig. 2(a) shows a typical trajectory for the reactive power compensation used to perform active voltage regulation. This figure shows how much reactive power should be injected as the voltage changes beyond the normal limits. In this figure, S_n is the rated apparent power (Volt-Amp) of the power converter and V_n is the rated grid voltage (e.g., 240 V for split-phase systems).

A. Active Power Control

The active power control gives the power converter the flexibility to adjust the output power based on the variations in the line frequency [34]. For example, an increase in the line frequency means that there is too much power. Thus, the power converter should reduce the power until the frequency reaches normal conditions. According to regulatory standards in North America (e.g., *UL1741*, and *IEEE 1547*), the frequency must remain between 59.2 and 60.6 Hz. Therefore, if the frequency reaches beyond the aforementioned limits, the power converter must be disconnected (islanded) from the utility grid [35]. However, as DG becomes more prevalent, it has a significant impact on the utility grid and the grid frequency can not be tightly fixed within the aforementioned limits [38]. Thus, local frequency regulation achieved by controlling the active power will soon be mandatory to be able to guarantee the stable operation of the DG system. Fig. 2(b) shows a typical trajectory for active power control. In this figure, $f_{\rm line}$ is the line frequency, f_n is the nominal frequency (e.g., 60 Hz in North America), and P_n is the rated power of the power converter. With this trajectory, the power converter can significantly mitigate the oversupply of power locally, leading to a more stable operating frequency.

B. Fault Ride-Through

As the share of renewable energy sources is growing exponentially, the capability of supporting the grid under fault/disturbance conditions is becoming essential. This capability, basically, enables the power converter to remain connected and supply reactive current to support the grid voltage during fault/disturbance conditions [39], [40].

Fig. 2(c) shows the fault ride-through profiles for a grid-connected power converter. According to these profiles, the power converter remains connected and supplies reactive power up to some point. In the event of a fault, the power converter continues to operate and support the grid by injecting reactive power, given that the voltage follows the expected profile shown in Fig. 2(c), until the voltage reaches a value in the normal range.

Considering the aforementioned discussion, the need for a fast and reliable active/reactive power closed-loop control system is inevitable in order to meet the emerging requirements for grid connection. In a practical HREGS, energy storage is required to effectively complement the intermittent renewable energy sources. Fig. 3 shows a power conditioning system for an energy storage unit used in residential/commercial applications. According to this figure, the power conditioning system includes two stages: a bidirectional ac/dc converter and a bidirectional dc/dc converter. The bidirectional ac/dc converter is usually a single-phase active rectifier and the bidirectional dc/dc converter

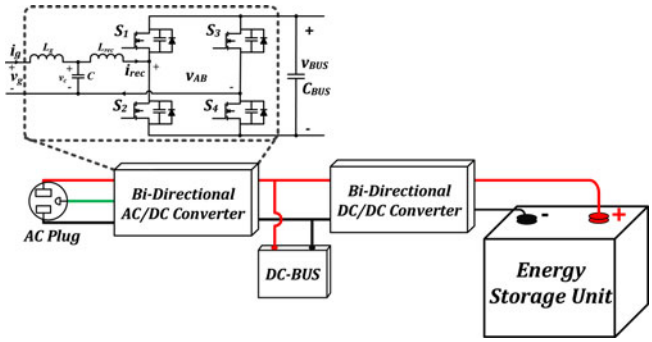

Fig. 3. Energy storage power conditioning system.

is commonly an isolated dual active bridge converter [41], [42]. There is an *LCL*-filter at the input of the active rectifier used in order to eliminate the high frequency harmonics [43]. An intermediate dc-bus is between the two stages and is needed in order to alternate the power ripple. According to Fig. 3, the active rectifier is the interface between the DG and the energy storage unit. The active rectifier control system should provide a fast and reliable closed-loop controller for active/reactive power control between the DG and the energy storage unit.

In the next section, a hybrid estimator is proposed, which is able to estimate the active and reactive power very quickly and reliably. The hybrid estimator is used in the closed-loop control system, which regulates active/reactive power in a single-phase power generation system for residential/commercial applications.

III. Proposed Hybrid Estimator for Active/Reactive Power Control

The control system of an ac/dc converter generally includes two external control loops, which determine the reference signal for the internal current loop. The two external control loops are the active power control loop and the reactive power control loop. The active power control loop usually regulates the dc-bus voltage in order to balance the active power flow [41]. This loop basically determines the amplitude of the current component aligned with the grid voltage. The reactive power control loop determines the quadrature current component (90° phase-shifted from the grid voltage). In this control system, the main difficulty is related to the active/reactive power calculation block, which feeds back the active power and reactive power signals to the closed-loop control system. In single-phase power conditioning systems, the extraction of the active power and reactive power requires a low-pass filter with a very low bandwidth. In a single-phase system, the instantaneous power is given by

$$p_{g,\text{inst}} = v_g i_g \tag{1}$$

where v_g is the grid voltage and i_g is the grid current. Let us consider the grid voltage and grid current to be as follows:

$$v_g = V\sin(\omega t) \tag{2}$$

$$i_g = I\sin(\omega t + \psi). \tag{3}$$

Thus, the instantaneous power is given by

$$p_{g,\text{inst}} = P - P\cos(2\omega t) + Q\sin(2\omega t) \tag{4}$$

where $P = V_{\text{rms}} I_{\text{rms}} \cos(\psi)$ is the active power, and $Q = V_{\text{rms}} I_{\text{rms}} \sin(\psi)$ is the reactive power.

According to (4), extracting P and Q from the feedback signals requires low-pass filtering with a very low bandwidth. This will result in very sluggish transient performance, and an inability to actively provide functions, such as active voltage regulation, active power control, and low voltage fault ride-through. In this section, a adaptive nonlinear estimator is presented, which is able to rapidly calculate the active and reactive power.

The objective of the proposed nonlinear adaptive estimator is to estimate P and Q from $p_{g,\text{inst}}$, which is given by (4), without significantly compromising the signals' dynamics. The state variables of the estimator are defined as

$$x_1 = p_{g,\text{inst}} \tag{5}$$

$$x_2 = \frac{1}{2\omega}\dot{x}_1. \tag{6}$$

According to (4), the estimator dynamics is derived as

$$\dot{X} = F.X + G.\theta \tag{7}$$

where

$$\theta = P, X = \begin{pmatrix} x_1 \\ x_2 \end{pmatrix}, F = \begin{pmatrix} 0 & 2\omega \\ -2\omega & 0 \end{pmatrix}, \text{ and } G = \begin{pmatrix} 0 \\ 2\omega \end{pmatrix}$$

In (7), $\theta = P$ is the unknown parameter. The problem in estimating θ is that θ appears in the second equation in (7), which determines the dynamics of x_2. Since x_2 is not measurable, it is not possible to estimate θ. The only observable state is $x_1 = p_{g,\text{inst}}$ (differentiating x_1 is not practical due to the noise amplification). Thus, the following change of variables is proposed to rectify this issue:

$$\begin{pmatrix} \xi_1 \\ \xi_2 \end{pmatrix} = \begin{pmatrix} 1 & 0 \\ -1 & 1 \end{pmatrix}\begin{pmatrix} x_1 \\ x_2 \end{pmatrix} + \begin{pmatrix} 0 \\ -1 \end{pmatrix}\theta. \tag{8}$$

The dynamics of the system with new variables is given by

$$\dot{\chi} = F'.\chi + G'.\theta \tag{9}$$

where

$$\chi = \begin{pmatrix} \xi_1 \\ \xi_2 \end{pmatrix}, F' = \begin{pmatrix} 2\omega & 2\omega \\ -4\omega & -2\omega \end{pmatrix}, \text{ and } G' = \begin{pmatrix} 2\omega \\ 0 \end{pmatrix}.$$

It is worthwhile to emphasize the importance of the change of variables given by (8). This change of variable makes the dynamics observable for the estimation of the dc-value. Therefore, it makes it possible to design an estimator for the dc-value. According to (9), the unknown variable θ appears in the measurable dynamics (i.e., $\dot{\xi}_1$). In the new coordinates the unknown variable θ is observable and the nonlinear adaptive observer is

given by

$$\begin{pmatrix} \dot{\hat{\xi}}_1 \\ \dot{\hat{\xi}}_2 \\ \dot{\hat{\theta}} \end{pmatrix} = \begin{pmatrix} 2\omega & 2\omega & 2\omega \\ -4\omega & -2\omega & 0 \\ 0 & 0 & 0 \end{pmatrix} \begin{pmatrix} \xi_1 \\ \hat{\xi}_2 \\ \hat{\theta} \end{pmatrix} + \begin{pmatrix} \alpha_1 \\ \alpha_2 \\ 2\gamma_1\omega \end{pmatrix} \tilde{\xi}_1 \tag{10}$$

where $\tilde{\xi}_1 = \xi_1 - \hat{\xi}_1$, and α_1, α_2, γ_1 are the observer gains.

According to (4), there are three coefficients in the expression for instantaneous power. The first coefficient represents the dc offset (P), the second coefficient represents the coefficient of the cosine function ($-P$), and the third coefficient represents the coefficient of the sine function (Q). By using (10) the only coefficient that can be estimated is the first coefficient, P. However, there are two more coefficients ($-P$ and Q) that should be estimated. The proposed estimator for these coefficients is designed as

$$\dot{\hat{P}} = -\gamma_2 \cos(2\omega t)\tilde{p}_{g,\text{inst}} \tag{11}$$

$$\dot{\hat{Q}} = \gamma_3 \sin(2\omega t)\tilde{p}_{g,\text{inst}} \tag{12}$$

$$\tilde{p}_{g,\text{inst}} = p_{g,\text{inst}} - [\hat{\theta} - \hat{P}\cos(2\omega t) - \hat{Q}\sin(2\omega t)]. \tag{13}$$

Therefore, the proposed hybrid estimator is given by

$$\dot{\hat{\xi}}_1 = 2\omega\xi_1 + 2\omega\hat{\xi}_2 + 2\omega\hat{\theta} + \alpha_1\tilde{\xi}_1 \tag{14}$$

$$\dot{\hat{\xi}}_2 = -4\omega\xi_1 - 2\omega\hat{\xi}_2 + \alpha_2\tilde{\xi}_1 \tag{15}$$

$$\dot{\hat{\theta}} = 2\omega\gamma_1\tilde{\xi}_1 \tag{16}$$

$$\tilde{p}_{g,\text{inst}} = p_{g,\text{inst}} - [\hat{\theta} - \hat{P}\cos(2\omega t) + \hat{Q}\sin(2\omega t)] \tag{17}$$

$$\dot{\hat{P}} = -\gamma_2 \cos(2\omega t)\tilde{p}_{g,\text{inst}} \tag{18}$$

$$\dot{\hat{Q}} = \gamma_3 \sin(2\omega t)\tilde{p}_{g,\text{inst}}. \tag{19}$$

The hybrid nonlinear adaptive estimator described by (14)–(19) is able to rapidly estimate the active power and reactive power in a single-phase power conditioning system. The block diagram of the proposed hybrid estimator is shown in Fig. 4. Using this estimator to extract the values of the active power and reactive power allows the active/reactive power control loops to have a very high bandwidth. Thus, the proposed estimator provides a practical solution to implement different real-time grid interconnection functionalities such as active voltage regulation, active power control and low voltage ride-through.

It is worthwhile to mention that the main difference between the proposed estimator and other adaptive observers is its hybrid structure, in the sense that the estimator includes two subestimators (as shown in Fig. 4). The first estimator is responsible for estimating θ, which is the active power, and then the estimated value $\hat{\theta}$ is fed to the second estimator, which estimates the active and reactive power values. This hybrid structure allows the estimator to produce a very robust and precise estimation. The hybrid structure also results in the global asymptotic stability of the estimator, as will be shown in Section V. When only a simple adaptive filtering algorithm (e.g., gradient descent, least mean square, etc.) is used to estimate the active and reactive power values, the stability and convergence of the estimator are not guaranteed and the estimator may produce inaccurate values for different operating conditions.

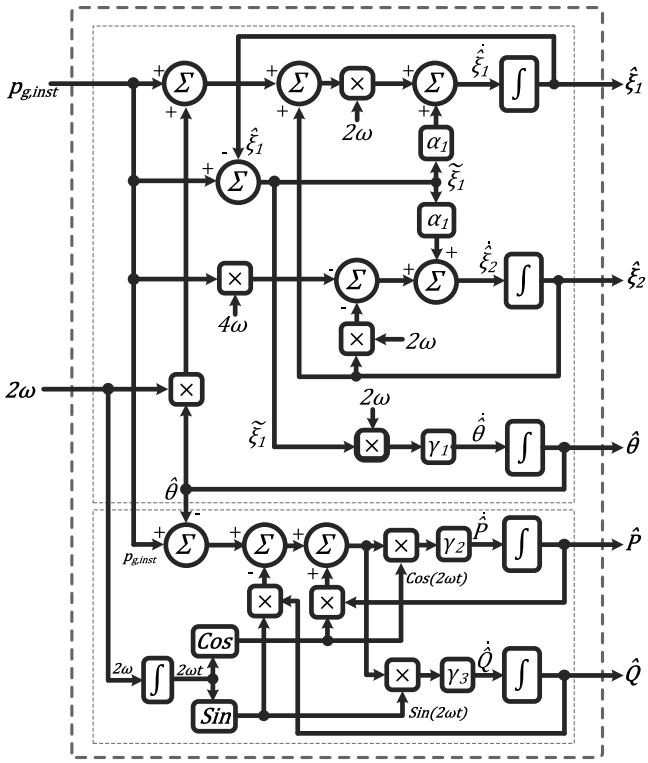

Fig. 4. Block diagram of the proposed hybrid nonlinear adaptive estimator.

IV. Active/Reactive Power Closed-Loop Control System

In the previous section a hybrid nonlinear adaptive estimator has been proposed, which is able to accurately and quickly estimate the active and reactive power. In this section, it is explained how this estimator fits into the energy storage unit control system. Fig. 5 shows the general block diagram of the control system for the energy storage unit. According to Fig. 5, the control system includes the ac/dc converter controller and the dc/dc converter controller. In order to have a practical energy storage unit with grid interconnection functionalities, reliable communication is essential between the control system and other components of the HREGS in a DG platform. Two common types of communication for this application are power line communication (PLC) and wireless RF-communication. PLC has been used in the industry for quite a long time. However, recently wireless communication has been given a lot of attention due to its flexibility and ease of integration. The capability of integrating the energy storage unit into the home automation systems is very desirable. In particular, Zigbee wireless communication has recently been used in several industrial products [44]–[46].

The ac/dc converter can operate either in autonomous mode or in nonautonomous mode. In autonomous mode, the reference values for the active power and reactive power are adaptively generated based on the grid condition detected by the ac/dc

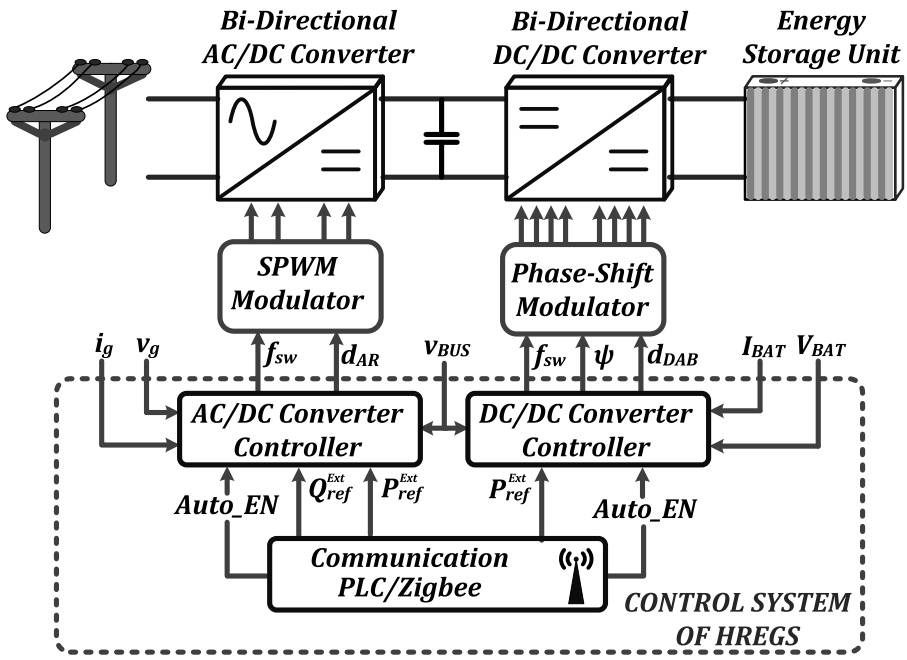

Fig. 5. Energy storage unit control system.

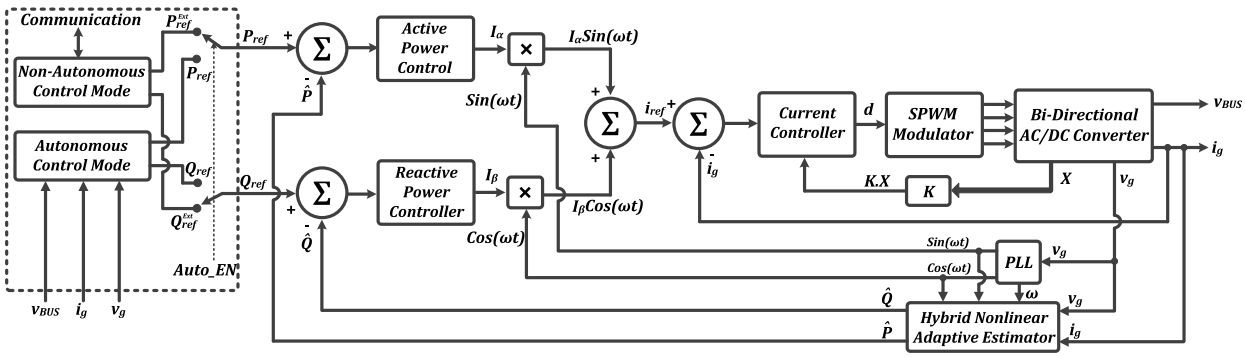

Fig. 6. Ac/dc converter closed-loop control system.

converter. Whereas, in the nonautonomous mode, the reference values for the active power and reactive power are determined by the communication unit. The operating mode can be set by the user based on the local grid conditions. The signal "*Auto_EN*" determines whether the control system operates in autonomous mode or nonautonomous mode.

Fig. 6 shows the ac/dc converter closed-loop control system in detail. According to this figure, the active power and reactive power are estimated through the proposed hybrid nonlinear adaptive estimator. The feedback signals are compared to the reference values for the active power and reactive power. The reference signals are produced either based on the grid conditions detected by the converter in autonomous mode, or externally from the communication unit. In autonomous mode, the main concern is mainly to provide active grid stabilization in a real-time manner. The main obligation in nonautonomous mode is to perform energy management. This is usually done through scheduled energy management. For instance, during the daytime when PV panels produce a lot of power, the energy management unit can store energy in the energy storage unit by peak shaving or power shifting. Then, during the evening the energy can be released from the energy storage unit based on the demand.

V. Stability Analysis of the Closed-Loop Control System

In this section the stability of the closed-loop control system is analysed. In particular, the stability of the proposed hybrid estimator as a component in the closed-loop control system is of interest. According to Fig. 6, the closed-loop control system includes an internal current loop, which is responsible for controlling the grid current, and an external power loop, which determines the reference value of the grid current such that the desired active and reactive power is tracked. The idea followed in this paper is to separate the stability analysis of the internal loop and external loop using singular perturbation theory

[60]–[64]. Then the stability of the hybrid estimator is analysed as a part of the external power loop. Singular perturbation theory is well suited for control systems that have state variables with different rates of change. This theory allows a typical nonlinear system to be broken down into subsystems with different time scales. Since the internal control loop is much faster than the external control loop, this theory can be applied to the closed-loop control system. The grid current control loop has much faster dynamics than the power control loop. The current control loop with fast dynamics is duly named the fast boundary layer and the power control loop with slow dynamics is named the slow quasi-steady state (these notations are based on the lexicon used in the singular perturbation theory [60]–[64]). In order to separate the dynamics of the system, some conditions should be satisfied. These conditions are laid out by the singular perturbation control theory and in particular Tikhonovs theorem [60]. This theorem states that for the system defined below

$$\frac{dx}{dt} = f(x,z,t) \tag{20}$$

$$\mu\frac{dz}{dt} = g(x,z,t) \tag{21}$$

the singular limit, $\mu = 0$, is used to obtain the following system:

$$\frac{dx}{dt} = f(x,z,t) \tag{22}$$

$$z = \phi(x,t) \tag{23}$$

where the second of these equations is the solution of $g(x,z,t) = 0$. (22), (23) are called a degenerate system. When μ converges to zero, the solution of the system (20), (21) tends to the solution of the degenerate system if $z = \phi(x,t)$ is a stable root of the adjoined system $\mu\frac{dz}{dt} = g(x,z,t)$.

The mathematical model of the grid-connected ac/dc converter with an *LCL*-filter is given by

$$\frac{di_g}{dt} = \frac{1}{L_g}v_g - \frac{1}{L_g}v_C \tag{24}$$

$$\frac{di_{\text{rec}}}{dt} = \frac{1}{L_{\text{rec}}}v_C - \frac{1}{L_{\text{rec}}}v_{AB} \tag{25}$$

$$\frac{dv_C}{dt} = \frac{1}{C}i_g - \frac{1}{C}i_{\text{rec}}. \tag{26}$$

According to (24)–(26) and Fig. 6, the fast dynamic is stable by choosing appropriate state-feedback $K.X$. Therefore, by using the Tikhonov's theorem, the stability analysis of the system can be narrowed down to the stability analysis of the external power loop. Intuitively, the fast dynamics given by (24)–(26) can be considered in their steady-state in the stability analysis of the external power loop according to Tikhonov's theorem.

The stability of the external power control loop depends on the hybrid estimator and the active and reactive power controllers. Again, the singular perturbation theory can be used to separate the stability analysis of the estimator and the controllers in the external power loop since the speed of the hybrid estimator is much faster than the controller by design. Therefore, the stability of the control system depends on the stability of the hybrid estimator. If the hybrid estimator is stable, the power controllers can be designed such that the stability of the closed-loop is guaranteed. Subsequently, the stability of the hybrid estimator is analyzed. In order to evaluate the stability of the proposed hybrid estimator, the error dynamics must be derived. According to (9)–(13), the error dynamics of the hybrid estimator is derived as (27) shown at the bottom of the page.

The stability analysis of the proposed hybrid estimator is performed using the Lyapunov stability theorem. The Lyapunov function is defined based on the error systems given by (27). Therefore, the Lyapunov function is given by

$$V = \frac{1}{2}\tilde{\xi}_1^2 + \frac{1}{2}\tilde{\xi}_2^2 + \frac{1}{2}\tilde{p}_{g,\text{inst}}^2 + \frac{1}{2\gamma_1}\tilde{\theta}_1^2 + \frac{1}{2\gamma_2}\tilde{P}^2 + \frac{1}{2\gamma_3}\tilde{Q}^2. \tag{28}$$

The derivative of the Lyapunov function is given by

$$\dot{V} = \tilde{\xi}_1\dot{\tilde{\xi}}_1 + \tilde{\xi}_2\dot{\tilde{\xi}}_2 + \tilde{p}_{g,\text{inst}}\dot{\tilde{p}}_{g,\text{inst}} + \frac{1}{\gamma_1}\tilde{\theta}_1\dot{\tilde{\theta}}_1 + \frac{1}{\gamma_2}\tilde{P}\dot{\tilde{P}} + \frac{1}{\gamma_3}\tilde{Q}\dot{\tilde{Q}}. \tag{29}$$

According to the error dynamics (27) and choosing the following coefficients:

$\alpha_1 \in \Re^+$, $\alpha_2 = 2\omega$, $\gamma_1 \in \Re^+$, $\gamma_2 = \gamma_3 = \gamma \in \Re^+$

the derivative of the Lyapunov function is derived as

$$\dot{V} = -\alpha_1\tilde{\xi}_1^2 - \alpha_2\tilde{\xi}_2^2 - \gamma\tilde{p}_{g,\text{inst}}^2 - 2\gamma_1\omega\tilde{p}_{g,\text{inst}}\tilde{\xi}_1 + \eta(\tilde{P},\tilde{Q},t)\tilde{p}_{g,\text{inst}} \tag{30}$$

where

$\eta(\tilde{P},\tilde{Q},t) = 2\omega[\tilde{P}(\cos(2\omega t) + \sin(2\omega t)) + \tilde{Q}(\cos(2\omega t) - \sin(2\omega t))]$.

By choosing $\gamma \gg |\bar{\eta}|$, $\alpha_1 > \gamma$, and $\gamma_1 = \frac{\gamma}{\omega}$, where, $|\bar{\eta}| = 4\omega(P_{\max} + Q_{\max})$ the derivative of the Lyapunov function is negative semidefinite. Therefore, the hybrid estimator can render the derivative of the Lyapunov function negative semidefinite. Therefore, only the stability (in the sense of boundedness)

$$\begin{pmatrix} \dot{\tilde{\xi}}_1 \\ \dot{\tilde{\xi}}_2 \\ \dot{\tilde{\theta}} \\ \dot{\tilde{p}}_{g,\text{inst}} \\ \dot{\tilde{P}} \\ \dot{\tilde{Q}} \end{pmatrix} = \begin{pmatrix} -\alpha_1 & 2\omega & 2\omega & 0 & 0 & 0 \\ -\alpha_2 & -2\omega & 0 & 0 & 0 & 0 \\ -2\gamma_1\omega & 0 & 0 & 0 & 0 & 0 \\ -2\gamma_1\omega & 0 & 0 & -(\gamma_2\cos^2(2\omega t) + \gamma_3\sin^2(2\omega t)) & 2\omega\sin(2\omega t) & 2\omega\cos(2\omega t) \\ 0 & 0 & 0 & \gamma_2\cos(2\omega t) & 0 & 0 \\ 0 & 0 & 0 & -\gamma_3\sin(2\omega t) & 0 & 0 \end{pmatrix} \begin{pmatrix} \tilde{\xi}_1 \\ \tilde{\xi}_2 \\ \tilde{\theta} \\ \tilde{p}_{g,\text{inst}} \\ \tilde{P} \\ \tilde{Q} \end{pmatrix} \tag{27}$$

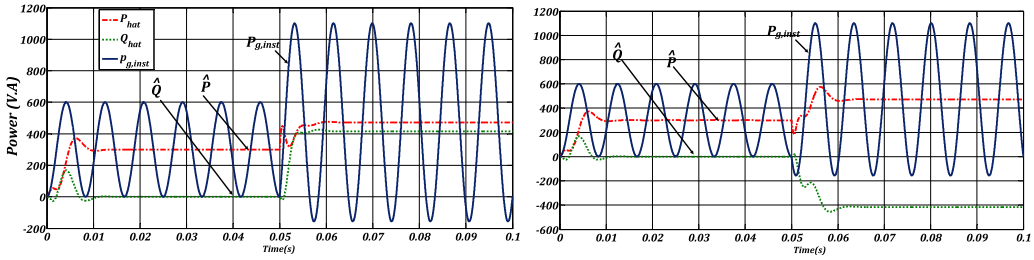

Fig. 7. Transient performance of the hybrid estimator.

of the error dynamics is guaranteed not the asymptotic stability [47]. Usually, when the derivative of the Lyapunov function is not negative-definite, LaSalle's invariance principle can be used to infer the asymptotic stability [48]–[50]. Using LaSalle's invariant set theorem, the set of points for which $\dot{V} = 0$ is determined. Then an invariant subset of this set is determined and it is shown that the error signals remain in this subset at all future times. LaSalle's invariant set theorem can not be applied to this particular system since the system is time-variant (nonautonomous) according to (27). For time-varying (nonautonomous) systems, Barbalat's Lemma can be used to analyze the asymptotic stability [51], [52]. Barbalat's Lemma states that if the time-variant Lyapunov function $\vartheta(t) = V(E(t))$, where $E(t) = (\tilde{\xi}_1, \tilde{\xi}_2, \tilde{p}^2_{g,\text{inst}}, \tilde{\theta}, \tilde{P}, \tilde{Q})$, satisfies the following conditions:

1) $\vartheta(t)$ is lower bounded,
2) $\dot{\vartheta}(t)$ is negative semidefinite,
3) $\dot{\vartheta}(t)$ is uniformly continuous in time (equivalently, $\ddot{\vartheta}(t)$ is finite),

then, $\vartheta(t) = V(E(t)) \longrightarrow 0$ as $t \longrightarrow 0$ (i.e., asymptotic stability of the error system).

According to (28)–(30), $\vartheta(t) = V(E(t))$ is lower bounded and negative semidefinite. In order to prove that $\vartheta(t)$ is uniformly continuous, $\ddot{\vartheta}(t)$ is calculated as follows:

$$\begin{aligned}\ddot{\vartheta}(t) = \; & (2\alpha_1^2 + 4\omega^2\gamma_1^2)\tilde{\xi}_1^2 - 4(\alpha_1 - \alpha_2)\omega\tilde{\xi}_1\tilde{\xi}_2 - 4\alpha_1\omega\tilde{\theta} \\ & + 4\alpha_2\omega\tilde{\xi}_2^2 + (2\omega\gamma_1\alpha_1 + 2\omega\gamma)\tilde{\xi}_1\tilde{p}_{g,\text{inst}} \\ & - 4\omega^2\gamma_1\tilde{\xi}_2\tilde{p}_{g,\text{inst}} - 4\omega^2\gamma_1\tilde{\theta}\tilde{p}_{g,\text{inst}} \\ & - 4\omega^2\gamma_1\sin(2\omega t)\tilde{\xi}_1\tilde{P} - 4\omega^2\gamma_1\cos(2\omega t)\tilde{\xi}_1\tilde{Q} \\ & + \dot{\eta}(\tilde{P}, \tilde{Q}, t)\tilde{p}_{g,\text{inst}} - 2\gamma_1\omega\tilde{\xi}_1\eta(\tilde{P}, \tilde{Q}, t) \\ & - \gamma\tilde{p}_{g,\text{inst}}\eta(\tilde{P}, \tilde{Q}, t) + 2\omega\sin(2\omega t)\tilde{P}\eta(\tilde{P}, \tilde{Q}, t) \\ & + 2\omega\cos(2\omega t)\tilde{Q}\eta(\tilde{P}, \tilde{Q}, t). \end{aligned} \tag{31}$$

All terms in the right-hand side of (31) are bounded. Thus, $\dot{\vartheta}(t)$ is uniformly continuous and according to Barbalat's Lemma $(\tilde{\xi}_1, \tilde{\xi}_2, \tilde{p}_{g,\text{inst}}) = (0, 0, 0)$ is the asymptotic stable equilibrium of the error dynamics.

(30), (31) and Barbalat's Lemma only prove the asymptotic stability of the error signals $(\tilde{\xi}_1, \tilde{\xi}_2, \tilde{p}_{g,\text{inst}})$. However, the convergence of the parameters $(\tilde{\theta}, \tilde{P}, \tilde{Q})$ have not been proven. In order to prove the convergence of the adaptive parameters to their actual values, the persistency of excitation (PE) theorem can be used [47]. This theorem states that if the update laws are persistently excited, global asymptotic stability is ensured for the estimation errors. In particular, in order to have persistency of excitation for a scalar function, $\phi(t)$, the following condition must be satisfied for two positive real values T and λ:

$$\int_t^{t+T} \phi^2(\tau)d\tau \geq \lambda > 0. \tag{32}$$

In single-phase power conditioning systems, due to the existence of the double-frequency harmonic, the condition of the PE theorem is usually satisfied. Therefore, this great advantage has been used in the proposed hybrid estimator in order to precisely estimate the active/reactive power. In particular, for the active and reactive power, the PE theorem's condition is satisfied according to (18) and (19). For the active power adaptive law (18), $\phi_P(t) = -\cos(2\omega t)$ and the PE theorem's condition is given by

$$\int_t^{t+\frac{2\pi}{\omega}} \cos^2(2\omega\tau)d\tau = \frac{\pi}{\omega} > 0. \tag{33}$$

Similarly, for the reactive power adaptive law (19), $\phi_Q(t) = \sin(2\omega t)$ and the PE theorem's condition is given by

$$\int_t^{t+\frac{2\pi}{\omega}} \sin^2(2\omega\tau)d\tau = \frac{\pi}{\omega} > 0. \tag{34}$$

According to (33), (34), the update laws in the proposed hybrid estimator are persistently excited. Therefore, the PE theorem proves the global asymptotic stability of the equilibrium point $(0, 0, 0)$ for $(\tilde{\theta}_1, \tilde{P}, \tilde{Q})$.

Fig. 7 shows the transient performance of the proposed hybrid estimator. This figure shows that it is able to estimate the active and reactive power very quickly (less than half a line cycle). The trajectory of the proposed hybrid estimator is illustrated in Fig. 8. Fig. 8 depicts how the system is steered from one steady-state condition to another with different active and reactive power values. Fig. 9 shows the limit cycles for the active and reactive power estimated by the proposed hybrid estimator.

According to the derivative of the Lyapunov function, the speed of the convergence for the active and reactive power is related to the coefficients, γ_1, γ_2, and, γ_3. According to Fig. 7, these coefficients can be adjusted to achieve very fast convergence of active and reactive power estimation.

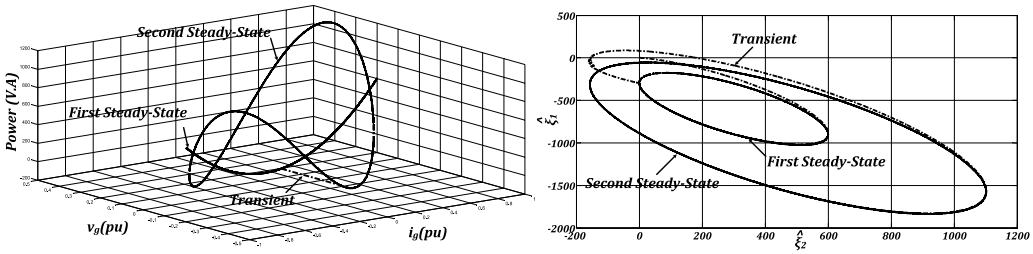

Fig. 8. Trajectory of the proposed hybrid estimator.

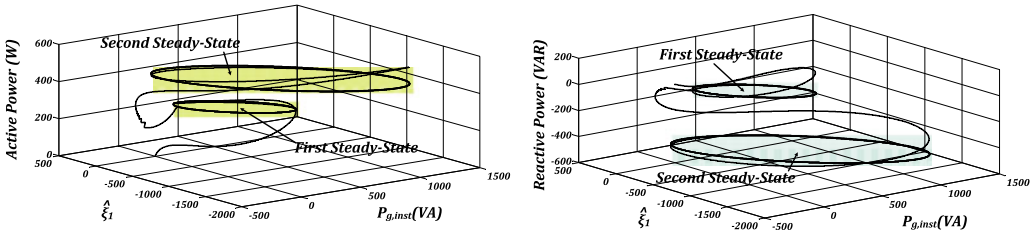

Fig. 9. Steady-state limit cycles of active power and reactive power.

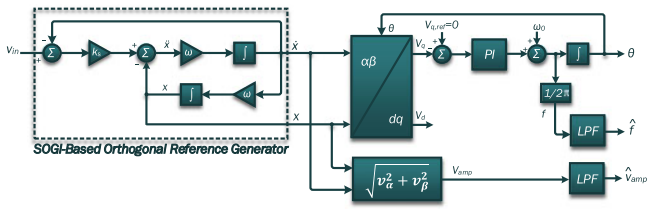

Fig. 10. SOGI-based PLL [68].

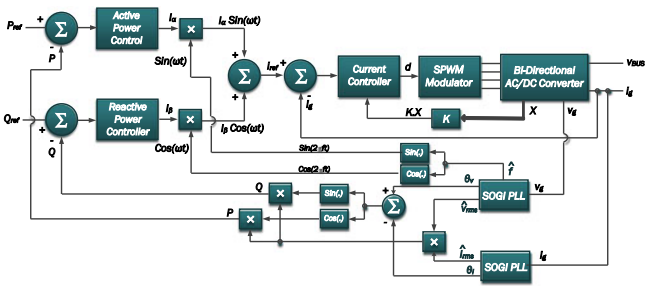

Fig. 11. Active/reactive power estimator using SOGI-based PLL.

VI. Comparative Study

In this section, the proposed hybrid estimator is compared to the state-of-the-art signal processing techniques used for this application. The intention is merely to shed some light on the advantages and disadvantages of the hybrid estimator compared to other methods. Most of the state-of-the-art signal processing techniques for grid-connected power converters are based on some type of orthogonal signal generation (OSG) [65]–[69]. The amplitude, phase, and frequency of the signal can easily be extracted using the respective orthogonal signals [68], [69]. In balanced three-phase system, the orthogonal signal generator is implemented by using the Clarke transformation [70]. However, in unbalanced conditions and single-phase systems, the orthogonal signal generator is not very straightforward. Among the state-of-the-art methods, the SOGI and ANF are commonly used for this application. Therefore, the performance of the proposed hybrid estimator is compared to that of the SOGI and the ANF. The SOGI has widely been used for grid synchronization [65]–[69].

Fig. 10 shows the block diagram of the SOGI-based phase-locked-loop (PLL). According to this figure, a SOGI is used to generate orthogonal signals. Then, the phase, frequency and amplitude of the signal are calculated using the orthogonal signals. This PLL can be used to estimate the active and reactive power for the power feedback signals. Fig. 11 shows the block diagram of the closed-loop control system using SOGI PLL to estimate active/reactive power. The advantages of this technique are the fairly fast and accurate signal processing capability and good noise rejection [66]. However, the use of the SOGI has some drawbacks; namely, the tuning of the passband width and the static centre frequency. Even though this technique provides a simple and practical solution for grid synchronization, it involves a rather complicated algorithm for measuring the active and reactive power due to the fact that the amplitudes and phases of both the voltage and current should be calculated. Also, if the grid frequency were to drift out of the passband, the SOGI would not be able to properly track the phase of the grid voltage without a leading or lagging effect. Adaptive variation of the coefficient ω is required to rectify this issue. That makes the digital implementation of this algorithm computationally intense. In addition, the SOGI is susceptible to the harmonic contents of the grid voltage and grid current. In order to mitigate the impact of harmonics, multiple modules should be implemented for different harmonics, which is called the MSOGI-FLL [65].

The second commonly used technique for grid synchronization is ANF [71]–[74]. Fig. 12 shows the block diagram of the ANF PLL. According to this figure, the ANF uses the SOGI

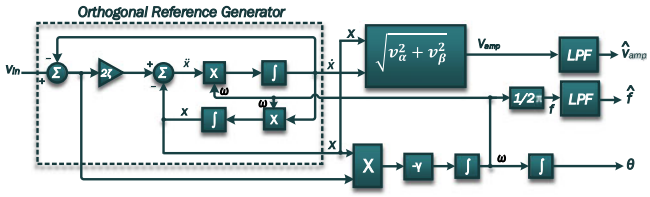

Fig. 12. ANF-based PLL [73].

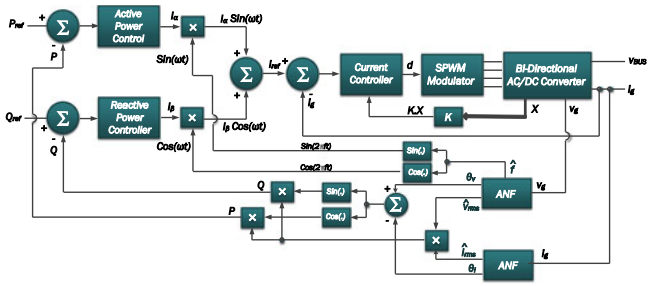

Fig. 13. Active/reactive power estimator using ANF-based PLL.

structure to produce the orthogonal signals. However, the ANF uses a different adaptive law to estimate the frequency/phase. Therefore, the ANF can adaptively track the grid frequency. Fig. 13 shows the block diagram of the closed-loop control system using an ANF to estimate the active and reactive power signals. This figure shows that the ANF blocks estimate the amplitude and phase of the grid voltage as well as the ones for the grid current. Therefore, the active and reactive power can be estimated using the extracted information. The ANF-based estimation has more or less the same difficulties as the SOGI technique. Also, both of these methods require low-pass filters for the output variables to produce smooth estimations. In addition, if there are dc offsets in the grid voltage or the grid current signals, the ANF and SOGI methods can not accurately estimate the power feedback signals.

Unlike the ANF and SOGI techniques, the proposed hybrid estimator does not use an orthogonal reference generator to process and reconstruct the signal. Therefore, it can mitigate the aforementioned disadvantages related to the ANF and SOGI techniques. The hybrid estimator performs the estimation in two consecutive stages. The first stage estimates $\hat{\theta}$, which is the dc value of the instantaneous power. Then $\hat{\theta}$ is used to estimate the active and reactive power. This double layer estimation creates robustness in the estimation. Also, it smooths out the final estimation. Thus, there is no need for low-pass filters at the output of the hybrid estimator. Fig. 14 shows the two-stage structure of the proposed hybrid estimator.

In terms of digital implementation the aforementioned three techniques have different levels of complexity. Therefore, the hybrid estimator is compared with the SOGI-based estimator and the ANF-based estimator in terms of digital implementation. Table I summarizes this comparison. According to Table I, the proposed hybrid observer requires more integrators as well as multipliers compared to the other two methods. However, with a resource sharing technique, the number of operators can be reduced significantly in the digital implementation [75]–[77].

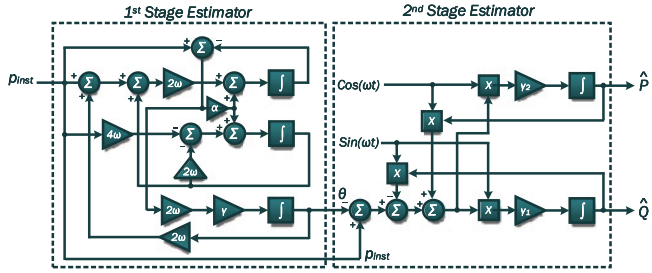

Fig. 14. Two-stage estimation of the proposed hybrid estimator block diagram.

TABLE I
COMPARISON IN TERMS OF DIGITAL IMPLEMENTATION

Operation	SOGI	ANF	Hybrid Estimator
Integrators	4	4	5
Multipliers	12	8	14
Add/Sub Blocks	9	5	9
LPFs	2	2	0
Trigonometric Functions	2	2	2

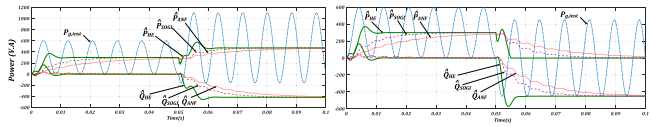

Fig. 15. Comparison of transient performance of the hybrid estimator, SOGI, and ANF.

TABLE II
AC/DC CONVERTER SIMULATION PARAMETERS

Symbol	Parameter	Value
P_{ratted}	Rated Power	3.2 kW
V_{BUS}	DC-Bus Voltage	400 – 450 VDC
v_g	Grid Voltage	208 – 246 VAC
f_{sAR}	Switching Frequency	20 kHz
L_{rec}	Rectifier Side Inductor	2.56 mH
R_{rec}	Rectifier Side Equivalent Resistance	35 mΩ
L_g	Grid Side Inductor	0.307 mH
R_g	Grid Side Equivalent Resistance	15 mΩ
C	*LCL*-Filter Capacitance	2.2 μF
C_{BUS}	DC-Bus Capacitor	470 μF

Fig. 15 illustrates the transient performance of three different estimators (hybrid estimator, SOGI estimator, and ANF estimator). This figure shows that the hybrid observer is able to quickly estimate the active and reactive power from the instantaneous power. Also, due to the double-layer estimation of the hybrid observer, the estimation results are very smooth compared to the SOGI and ANF, which usually require a moving average filter to remove the ripple.

VII. PERFORMANCE ANALYSIS THROUGH SIMULATION

In this section, the performance of the proposed active/reactive power controller is evaluated through computer simulations. Table II contains the ac/dc converter specifications used to conduct the simulations for the closed-loop control system.

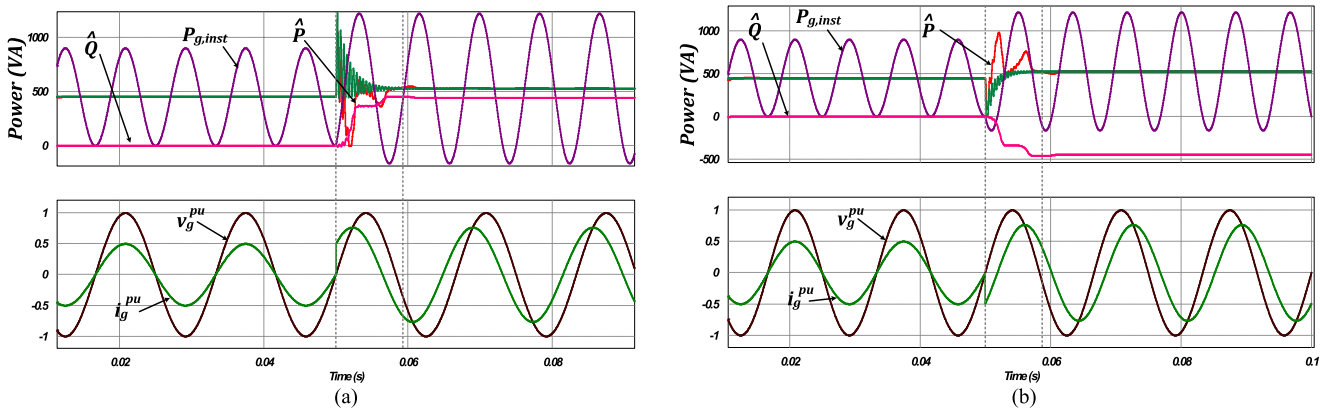

Fig. 16. Transient performance of the proposed hybrid estimator for different step changes in active and reactive power. (a) 50 W step change in active power, 450 VAR step change in reactive power, (b) 50 W step change in active power, −450 VAR step change in reactive power.

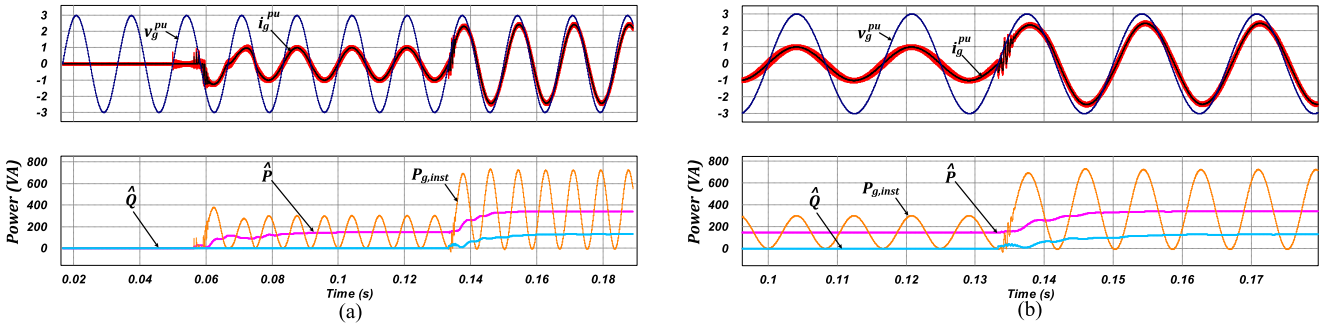

Fig. 17. Transient response of the closed-loop control system.

The simulations in this section are conducted using PowerSim V.9.3.2.

Fig. 16 illustrates the transient performance of the proposed hybrid estimator for different step changes in the active and reactive power. This figure depicts the transient response when a 50 W step change in the active power and ±450 VAR step change in the reactive power are applied. It should be noted that the grid current and grid voltage shown in Fig. 16 are the corresponding sampled values. This figure shows the very fast and accurate estimation of the active and reactive power performed by the proposed hybrid estimator. Fig. 17 shows the performance of the closed-loop control system of the ac/dc converter when the feedback signals for the active and reactive power are estimated by the proposed hybrid estimator. Fig. 17 shows the stable operation of the closed-loop control system. In Fig. 18, the performance of the hybrid estimator against harmonics is evaluated. In this figure, 7% of the third harmonic, 5% of the fifth harmonic and 3% of the seventh harmonic have been applied to the grid current. This figure shows that the hybrid estimator can compensate the error caused by the harmonics through the instantaneous power error $\hat{p}_{\text{inst}}$. It should be noted that the aforementioned harmonics are applied to the grid current waveform. The hybrid estimator shows the same performance for the voltage harmonics since it processes the instantaneous power. Fig. 19 shows the performance of the hybrid estimator when

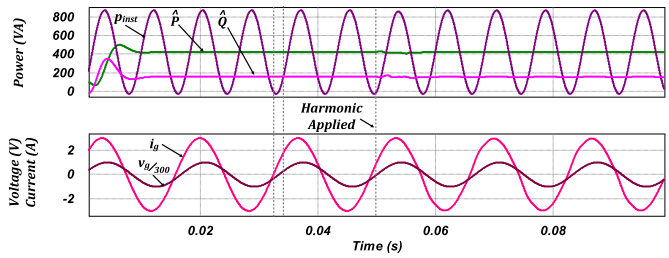

Fig. 18. Response of the hybrid estimator against harmonics (seventh-harmonic:3%, fifth-harmonic: 5%, third-harmonic: 7%).

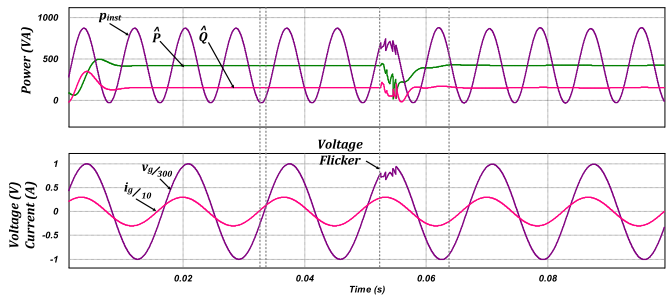

Fig. 19. Response of the hybrid estimator against voltage flickers.

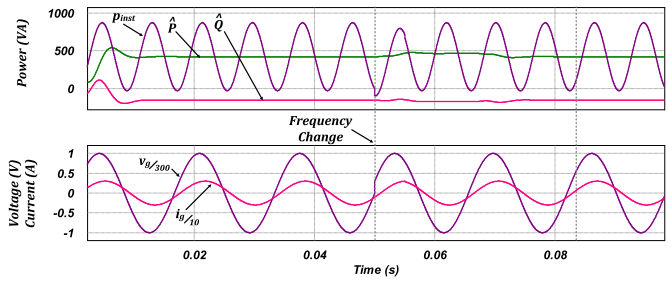

Fig. 20. Response of the hybrid estimator against line frequency change.

TABLE III
SPECIFICATIONS OF AC/DC CONVERTER EXPERIMENTAL PROTOTYPE

Symbol	Parameter	Value
P	Power	3.2 kW
V_{BAT}	Battery Voltage	$235-430$ V
I_{BAT}	Battery Maximum Charging Current	10 A
v_g	Grid Voltage	$208-246$ V
i_g	Rated Grid Current	$16A$
f_{sAR}	Switching Frequency	20 kHz
L_{rec}	Rectifier Side Inductor	2.56 mH
R_{rec}	Rectifier Side Equivalent Resistance	35 mΩ
L_g	Grid Side Inductor	0.307 mH
R_g	Grid Side Equivalent Resistance	15 mΩ
C	*LCL*-Filter Capacitance	2.2 μF
C_{BUS}	DC-Bus Capacitor	470 μF

the grid voltage is subject to flickers. According to this figure the hybrid estimator is able to recover the estimated values very quickly. The performance of the hybrid estimator when there is a change in line frequency is depicted in Fig. 20. In this figure, the line frequency changes from 60 to 61.1 Hz. The grid frequency is tracked by the PLL and is given to the hybrid estimator. This structure creates another level of robustness against noise, since the PLL generates a clean frequency estimation and inserts it into the hybrid estimator.

VIII. EXPERIMENTAL RESULTS

An experimental prototype of an ac/dc converter has been implemented in order to evaluate the performance of the proposed active/reactive power control method. The specifications of the implemented ac/dc converter are given in Table III.

The control system is implemented using a field-programmable gate array (FPGA). FPGAs are able to provide a very fast and reliable solution to digitally implement the proposed control system. In particular, the Cyclone IV $EP4CE22F17C6N$ from Altera is used to implement the control system. This FPGA provides a very fast and cost-effective solution for the control of power converters. Different control loops are implemented using VHSIC hardware description language (VHDL). The control loops in VHDL codes are based on the new IEEE "fixed-point" library, which is supported by VHDL-2008 compilers [53], [54].

Fig. 21 shows the block diagram of the digital control system implemented by the FPGA for the ac/dc converter. According to this figure, the communication system provides the reference values for the active power and reactive power in the nonautonomous mode of operation. The energy management unit decides the mode of operation based on the grid conditions and the signals produced by the communication system. Once the reference values for the active and reactive power have been determined, the active/reactive power controller produces the reference signal for the grid current based on the reference values and the active and reactive power feedback signals estimated by the proposed hybrid estimator. Then the internal current loop controls the grid current accordingly.

Using FPGAs in implementing the control loops has recently been very popular due to the speed and reliability that they provide in implementing complex control algorithms [55]–[58]. In order to implement the proposed hybrid estimator by the FPGA, the equations of the hybrid estimator must be discretized. The equations of hybrid estimator in the discrete format are given by

$$\begin{aligned}\hat{\xi}_1[n] = {} & \hat{\xi}_1[n-1] + \omega T_s \xi_1[n] + \omega T_s \hat{\xi}_2[n] + \omega T_s \hat{\theta}[n] \\ & + \frac{T_s}{2}\alpha_1 \tilde{\xi}_1[n] + \omega T_s \xi_1[n-1] + \omega T_s \hat{\xi}_2[n-1] \\ & + \omega T_s \hat{\theta}[n-1] + \frac{T_s}{2}\alpha_1 \tilde{\xi}_1[n-1] \qquad (35)\end{aligned}$$

$$\begin{aligned}\hat{\xi}_2[n] = {} & \hat{\xi}_2[n-1] - 2\omega T_s \xi_1[n] - \omega T_s \hat{\xi}_2[n] \tilde{\xi}_1[n] \\ & + \frac{T_s}{2}\alpha_2 - 2\omega T_s \xi_1[n-1] \\ & - \omega T_s \hat{\xi}_2[n-1] + \frac{T_s}{2}\alpha_2 \tilde{\xi}_1[n-1] \qquad (36)\end{aligned}$$

$$\hat{\theta}[n] = \hat{\theta}[n-1] + \omega T_s \gamma_1 \tilde{\xi}_1[n] + \omega T_s \gamma_1 \tilde{\xi}_1[n-1] \qquad (37)$$

$$\begin{aligned}\tilde{p}_{g,\text{inst}}[n] = {} & p_{g,\text{inst}}[n-1] - \{\hat{\theta}[n] - \hat{P}[n]\cos(2\omega n T_s) \\ & + \hat{Q}[n]\sin(2\omega n T_s)\} \qquad (38)\end{aligned}$$

$$\begin{aligned}\hat{P}[n] = {} & \hat{P}[n-1] - \frac{T_s}{2}\gamma_2 \cos(2\omega n T_s)\tilde{p}_{g,\text{inst}}[n] \\ & - \frac{T_s}{2}\gamma_2 \cos(2\omega(n-1)T_s)\tilde{p}_{g,\text{inst}}[n-1] \qquad (39)\end{aligned}$$

$$\begin{aligned}\hat{Q}[n] = {} & \hat{Q}[n-1] + \frac{T_s}{2}\gamma_3 \sin(2\omega n T_s)\tilde{p}_{g,\text{inst}}[n] \\ & + \frac{T_s}{2}\gamma_3 \sin(2\omega n - 1T_s)\tilde{p}_{g,\text{inst}}[n-1]. \qquad (40)\end{aligned}$$

The coefficients of the hybrid estimator should be designed such that the estimator has a much faster convergence speed compared to the power controllers bandwidth. According to Fig. 14, α and γ determine the speed of the first stage of the hybrid estimator, and γ_1 and γ_2 define the speed of the second stage of the hybrid estimator. The coefficients α and γ are chosen to produce a more aggressive response for the estimation, and the coefficients γ_1 and γ_2 are selected to produce a smooth estimation of the active and reactive power. Table IV shows the selected values for these coefficients in the experimental implementation.

According to (35)–(40), the digital implementation of the proposed hybrid estimator requires five integrators compared to

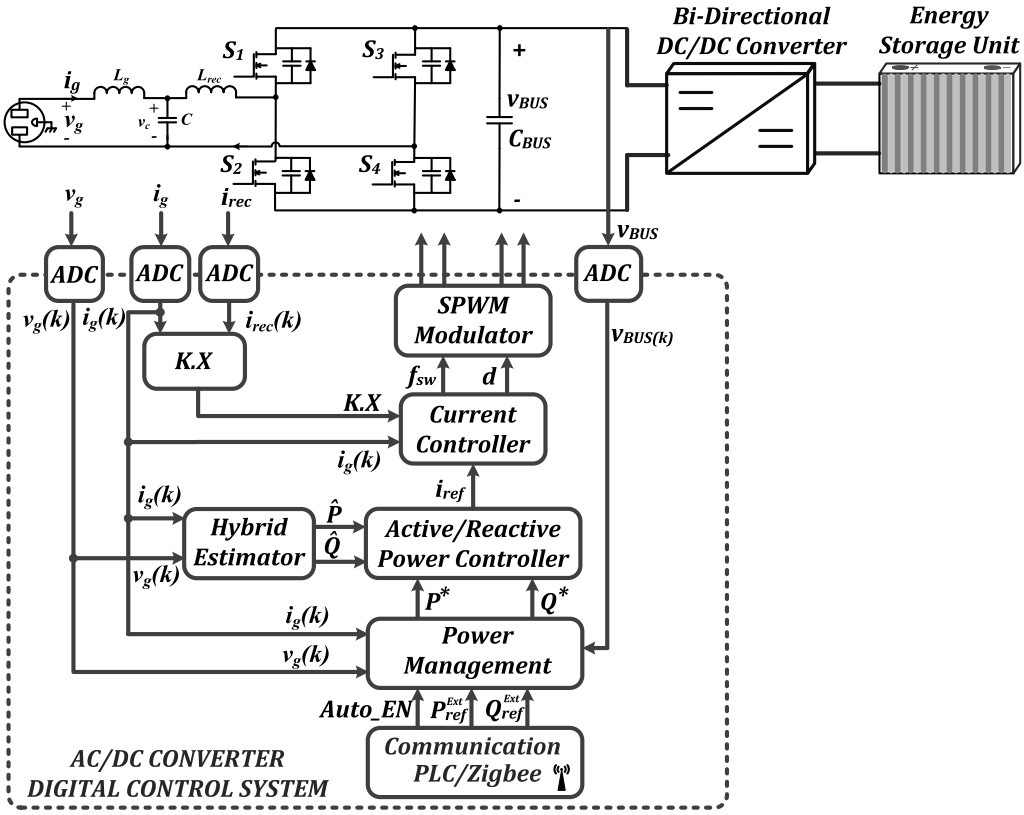

Fig. 21. Block diagram of the ac/dc converter digital control system.

TABLE IV
HYBRID OBSERVER COEFFICIENTS

Symbol	Parameter	Value
α	$\hat{p}_{\rm inst}$ coefficient	365
γ	$\hat{\theta}$ coefficient	235
γ_1	$\hat{P}$ coefficient	125
γ_2	$\hat{Q}$ coefficient	125

the conventional dq-transformation technique, which needs four integrators for digital implementation (two for the orthogonal generator and one for the PI controller and one for the phase angle). Also, the proposed hybrid estimator requires a fairly high number of digital multipliers (14 multipliers) compared to the conventional dq-transformation technique (nine multipliers). However, the number of required multipliers can be reduced drastically by using a "Resource Sharing" technique in digital implementation [75]–[77]. With resource sharing, one multiplier can be used for different operations. However, special care has to be taken in terms of timing in order to achieve a reliable solution with simple digital implementation.

Fig. 22 shows the experimental waveforms of the ac/dc converter when the converter only draws active power from the utility grid. This figure shows different waveforms such as the inverter voltage, v_{AB}, the grid voltage, v_g, the grid current, i_g, and the *LCL* second inductor current, $i_{\rm rec}$. Experimental waveforms when the ac/dc converter processes both active and reactive power are shown in Fig. 23. Fig. 24 illustrates the experimental results when the ac/dc converter performs reactive power compensation.

In this particular design, an integrated Zigbee transceiver module is used to establish communication for the ac/dc converter. The Zigbee module is the "*ZICM357SP2*" module from California Eastern Laboratories, which can accommodate diverse range and performance requirements [59]. Also, it can easily be integrated into home automation devices. This module uses the Ember *EM35x* RF transceiver and an *ARM CORTEX-M3* microcontroller. It also includes a power amplifier and a switch. Through this Zigbee module, the energy storage power conditioning system communicates with other devices in the smart grid platform.

The transient performance of the proposed control system of the energy storage power conditioning system is shown in Figs. 25–28. In particular, Figs. 25 and 26, respectively, show the transient performance of the converter when step changes of ± 1200 VAR (lag) and ± 1800 VAR (lag) are applied. These figures demonstrate the lagging power factor (i.e., the grid current is lagging the grid voltage). Fig. 27 shows the transient performance of the converter when a step change of ± 1200 VAR leading reactive power is applied. Fig. 28 demonstrates the transient performance of the energy storage power conditioning system when the power charged in the battery is released to the grid. This figure shows the transient performance for a step change of ± 1200 VAR. According to the transient performance

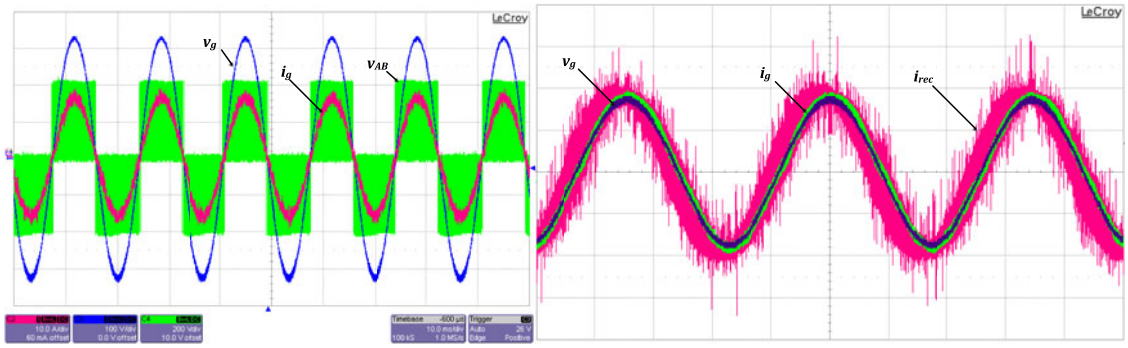

Fig. 22. Experimental waveforms of the ac/dc converter when the converter only draws active power from the grid (steady-state).

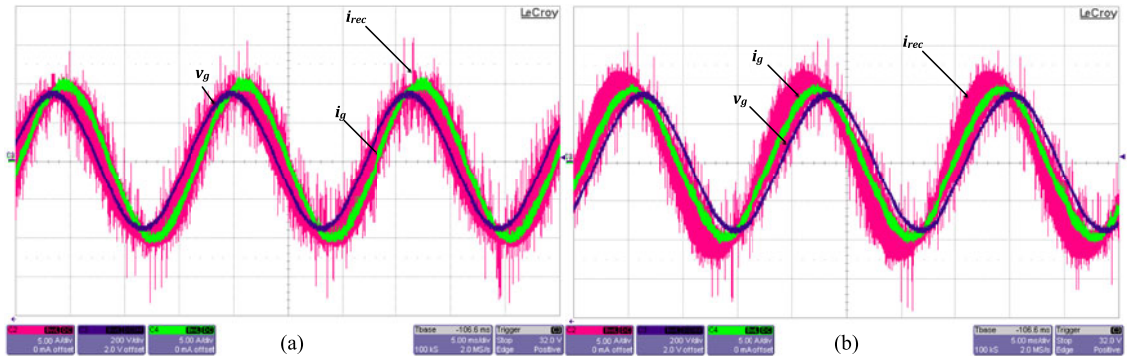

Fig. 23. Experimental waveforms of the ac/dc converter when the converter processes active and reactive power (steady-state).

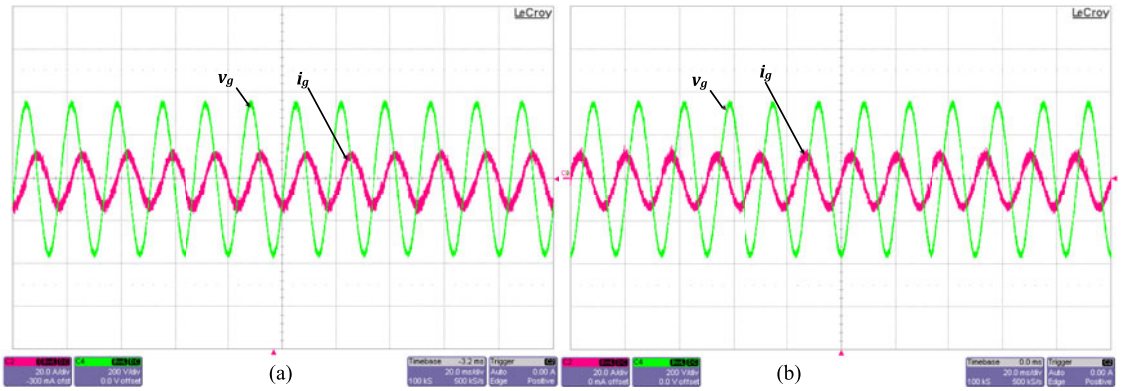

Fig. 24. Experimental waveforms of the ac/dc converter when the converter performs reactive power compensation (steady-state).

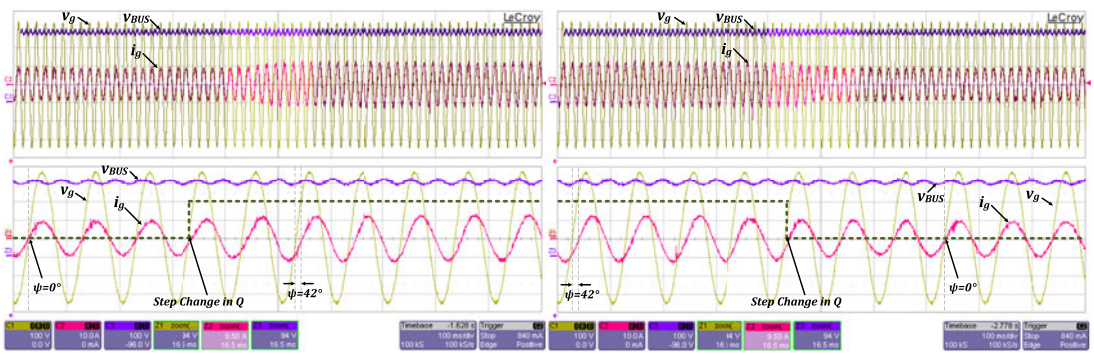

Fig. 25. Experimental waveforms of the ac/dc converter when a step change of ± 1200 VAR (lag) is applied (transient).

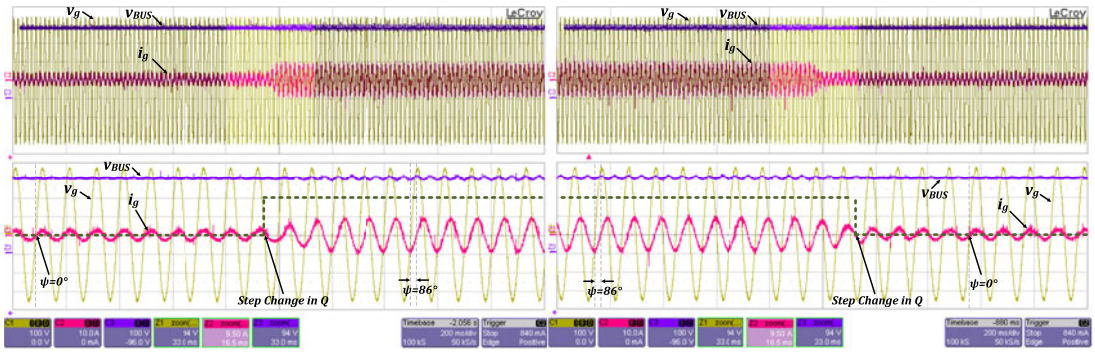

Fig. 26. Experimental waveforms of the ac/dc converter when a step change of $\pm$1800 VAR (lag) is applied (transient).

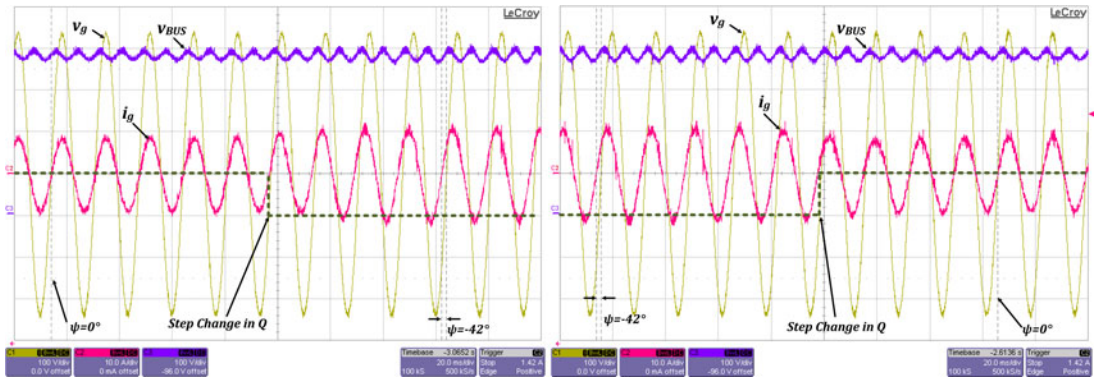

Fig. 27. Experimental waveforms of the ac/dc converter when a step change of $\pm$1200 VAR (lead) is applied (transient).

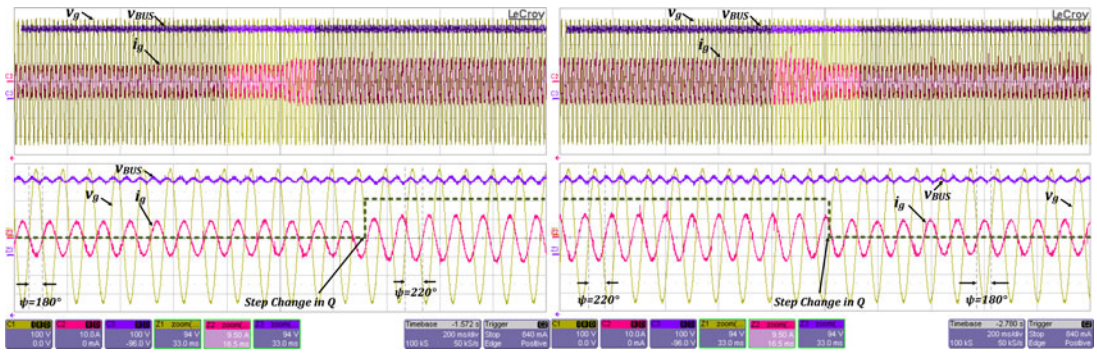

Fig. 28. Experimental waveforms of the ac/dc converter when a step change of $\pm$1200 VAR is applied (transient).

of the energy storage power conditioning system shown in Figs. 25–28, it can be concluded that the proposed active/reactive power closed-loop control system can provide very robust and fast transient performance for the energy storage system, leading to the reliable integration of the energy storage system into the smart grid.

The capability of supporting the grid under fault/disturbance conditions is illustrated in Fig. 29. This figure shows the performance of the converter when the grid voltage collapses for some reason (e.g., transients during active/reactive load changes). In the normal conditions, the converter should be disconnected from the utility grid (i.e., islanding condition). However, the proposed closed-loop control system can provide low voltage ride through capability and still support the grid under low voltage fault. According to Fig. 29 when the grid voltage collapses, the closed-loop control system performs reactive power compensation as well as active power control in order to support the grid under faulty conditions.

IX. Conclusion

As renewable energy sources replace conventional power generation systems, they will be required to perform more sophisticated functions, such as active voltage regulation, active power control, and fault ride-through. The future HREGSs, which will combine wind and solar energy with an energy storage unit for

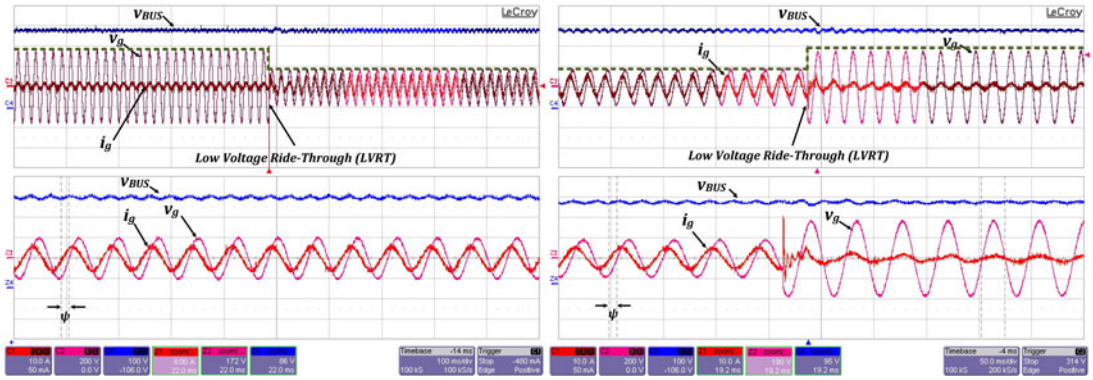

Fig. 29. Experimental waveforms for low voltage ride through.

commercial/residential applications, should be able to perform grid functionalities in a DG platform. A hybrid estimator has been proposed to quickly and accurately estimate the active power and reactive power values for the closed-loop control system of an HREGS. This fast estimation enables the HREGS to perform active/reactive power control in a real-time manner. Therefore, the proposed hybrid estimator can be an integral part of the closed-loop control system for future HREGSs. Simulation and experimental results validate the improved performance of the proposed closed-loop control system.

REFERENCES

[1] M. Liserre, T. Sauter, and J. Y. Hung, "Future energy systems: Integrating renewable energy sources into the smart power grid through industrial electronics," *IEEE Ind. Electron. Mag.,* vol. 4, no. 1, pp. 18–37, Mar. 2010.

[2] B. K. Bose, "Global energy scenario and impact of power electronics in 21st century," *IEEE Trans. Ind. Electron.*, vol. 60, no. 7, pp. 2638–2651, Jul. 2013.

[3] F. Blaabjerg, Z. Chen, and S. B. Kjaer, "Power electronics as efficient interface in dispersed power generation systems," *IEEE Trans. Power Electron.*, vol. 19, no. 5, pp. 1184–1194, Sep. 2004.

[4] A. Jamehbozorg and G. Radman, "Small signal analysis of power systems with wind and energy storage units," *IEEE Trans. Power Syst.*, vol. 30, no. 1, pp. 298–305, Jan. 2015.

[5] L. S. Vargas, B.-G. Turu, and F. Larrain, "Wind power curtailment and energy storage in transmission congestion management considering power plants ramp rates," *IEEE Trans. Power Syst.*, to be published.

[6] Q. Jiang, Y. Gong, and H. Wang, "A battery energy storage system dual-layer control strategy for mitigating wind farm fluctuations," *IEEE Trans. Power Syst.*, vol. 28, no. 3, pp. 3263–3273, Aug. 2013.

[7] S. Y. Derakhshandeh, A. S. Masoum, S. Deilami, M. A. S. Masoum, and M. E. H. Golshan, "Coordination of generation scheduling with PEVs charging in industrial microgrids," *IEEE Trans. Power Syst.*, vol. 28, no. 3, pp. 3451–3461, Aug. 2013.

[8] M. Yilmaz and P. T. Krein, "Review of battery charger topologies, charging power levels, and infrastructure for plug-in electric and hybrid vehicles," *IEEE Trans. Power Electron.*, vol. 28, no. 5, pp. 2151–2169, May 2013.

[9] R. Sioshansi and P. Denholm, "Emissions impacts and benefits of plug-in hybrid electric vehicles and vehicle-to-grid services," *Environ. Sci. Technol.*, vol. 43, no. 4, pp. 1199–1204, Feb. 2009.

[10] C. Thomas, "Fuel cell and battery electric vehicles compared," *Int. J. Hydrogen Energy*, vol. 34, no. 15, pp. 6005–6020, Aug. 2009.

[11] M. Yilmaz and P. T. Krein, "Review of the impact of vehicle-to-grid technologies on distribution systems and utility interfaces," *IEEE Trans. Power Electron.*, vol. 28, no. 12, pp. 5673–5689, Dec. 2013.

[12] S. Mischinger, W. Hennings, and K. Strunz, "Integration of surplus wind energy by controlled charging of electric vehicles," in *Proc. Innovative Smart Grid Technol. Int. Conf. Exhib.*, Oct. 2012, pp. 1–7.

[13] B. Kramer, S. Chakraborty, and B. Kroposki, "A review of plug-in vehicles and vehicle-to-grid capability," in *Proc. Ind. Electron. Annu. Conf.*, Nov. 2008, pp. 2278–2283.

[14] M. C. Kisacikoglu, B. Ozpineci, L. M. Tolbert, and F. Wang, "Single-phase inverter design for V2G reactive power compensation," in *Proc. Appl. Power Electron. Conf. Expo.*, Mar. 2011, pp. 808–814.

[15] D. Q. Xu, G. Joos, M. Levesque, and M. Maier, "Integrated V2G, G2V, and renewable energy sources coordination over a converged fiber-wireless broadband access network," *IEEE Trans. Smart Grid*, vol. 4, no. 3, pp. 1381–1390, Sep. 2013.

[16] M. Yilmaz and P. T. Krein, "Review of the impact of vehicle-to-grid technologies on distribution systems and utility interfaces," *IEEE Trans. Power Electron.*, vol. 28, no. 12, pp. 5673–5689, Dec. 2013.

[17] P. Mitra and G. K. Venayagamoorthy, "Wide area control for improving stability of a power system with plug-in electric vehicles," *IET Generation, Transmiss. Distrib.,*vol. 4, no. 10, pp. 1151–1163, Oct. 2010.

[18] M. D. Galus, R. A. Waraich, F. Noembrini, K. Steurs, G. Georges, K. Boulouchos, K. W. Axhausen, and G. Andersson, "Integrating power systems, transport systems and vehicle technology for electric mobility impact assessment and efficient control," *IEEE Trans. Smart Grid*, vol. 3, no. 2, pp. 934–949, Jun. 2012.

[19] A. Molderink, V. Bakker, M. G. C. Bosman, J. L. Hurink, and G. J. M. Smit, "Management and control of domestic smart grid technology," *IEEE Trans. Smart Grid*, vol. 1, no. 2, pp. 109–119, Sep. 2010.

[20] X. Fang, S. Misra, G. Xue, and D. Yang, "Smart grid: The new and improved power grid: A survey," *IEEE Commun. Surveys Tutorials*, vol. 14, no. 4, pp. 944–980, Oct.–Dec. 2012.

[21] F. Blaabjerg, R. Teodorescu, M. Liserre, and A. V. Timbus, "Overview of control and grid synchronization for distributed power generation systems," *IEEE Trans. Ind. Electron.*, vol. 53, no. 5, pp. 1398–1409, Oct. 2006.

[22] J. M. Guerrero, L. Hang, and J. Uceda, "Control of distributed uninterruptible power supply systems," *IEEE Trans. Ind. Electron.*, vol. 55, no. 8, pp. 2845–2859, Aug. 2008

[23] Y. Xue, L. Chang, S. B. Kjaer, J. Bordonau, and T. Shimizu, "Topologies of single-phase inverters for small distributed power generators: an overview," *IEEE Trans. Power Electron.*, vol. 19, no. 5, pp. 1305–1314, Sep. 2004.

[24] Y. Yang and F. Blaabjerg, "A new power calculation method for single-phase grid-connected systems," in *Proc. Ind. Electron. IEEE Int. Symp.*, May 2013, pp. 1–6.

[25] H. Akagi, E. H. Watanabe, and M. Aredes, *Instantaneous Power Theory and Applications to Power Conditioning*. New York, NY, USA: Wiley, 2007.

[26] R. Zhang, M. Cardinal, P. Szczesny, and M. Dame, "A grid simulator with control of single-phase power converters in DQ rotating frame," in *Proc. Power Electron. Spec. Conf.*, Jun. 2002, vol. 3, pp. 1421–1436.

[27] N. Akel, M. Pahlevaninezhad, and P. Jain, "A D-Q rotating frame reactive power controller for single-phase bi-directional converters," in *Proc. Telecommun. Energy Conf.*, 2014, pp. 1–5.

[28] M. Saitou and T. Shimizu, "Generalized theory of instantaneous active and reactive powers in single-phase circuits based on Hilbert transform," in *Proc. Power Electron. Spec. Conf.,* 2002, pp. 1419–1424.

[29] C. Subramanian and R. Kanagaraj, "Single-phase grid voltage attributes tracking for the control of grid power converters," *IEEE J. Emerg.*

Sel. Topics Power Electron., vol. 2, no. 4, pp. 1041–1048, Dec. 2014.
[30] M. Ciobotaru, V. G. Agelidis, R. Teodorescu, and F. Blaabjerg, "Accurate and less-disturbing active antiislanding method based on PLL for grid-connected converters," *IEEE Trans. Power Electron.*, vol. 25, no. 6, pp. 1576–1584, Jun. 2010.
[31] E. T. Andrade, P. E. M. J. Ribeiro, J. O. P. Pinto, C. L. Chen, J. S. Lai, and N. Kees, "A novel power calculation method for droop-control microgrid systems," in *Proc. Appl. Power Electron. Conf. Expo.*, Feb. 2012, pp. 2254–2258.
[32] J. M. Guerrero, L. G. De Vicuna, J. Matas, M. Castilla, and J. Miret, "A wireless controller to enhance dynamic performance of parallel inverters in distributed generation systems," *IEEE Trans. Power Electron.*, vol. 19, no. 5, pp. 1205–1213, Sep. 2004.
[33] M. A. Abusara, J. M. Guerrero, and S. M. Sharkh, "Line-interactive UPS for microgrids," *IEEE Trans. Ind. Electron.*, vol. 61, no. 3, pp. 1292–1300, Mar. 2014.
[34] Q. Shafiee, J. M. Guerrero, and J. C. Vasquez, "Distributed secondary control for islanded microgrids: A novel approach," *IEEE Trans. Power Electron.*, vol. 29, no. 2, pp. 1018–1031, Feb. 2014.
[35] *Inverters, Converters, Controllers and Interconnection System Equipment for Use With Distributed Energy Resources*, UL1741 Standard, Jan. 2010.
[36] *Standard for Interconnecting Distributed Resources With Electric Power Systems*, IEEE 1547, Jul. 2003.
[37] *IEEE Standard Conformance Test Procedures for Equipment Interconnecting Distributed Resources With Electric Power Systems*, Jul. 2005.
[38] *Recommendations for Updating the Technical Requirements for Inverters in Distributed Energy Resources*, Rule 21, Jan. 2014.
[39] P. Rodriguez, A. V. Timbus, R. Teodorescu, M. Liserre, and F. Blaabjerg, "Flexible active power control of distributed power generation systems during grid faults," *IEEE Trans. Ind. Electron.*, vol. 54, no. 5, pp. 2583–2592, Oct. 2007.
[40] M. Mirhosseini, J. Pou, and V. G. Agelidis, "Single- and two-stage inverter-based grid-connected photovoltaic power plants with ride-through capability under grid faults," *IEEE Trans. Sustainable Energy*, vol. 6, no. 3, pp. 1150–1159, Jul. 2015.
[41] M. Pahlevaninezhad and P. Jain, "A fast DC-bus voltage controller for bi-directional single-phase AC/DC converters," *IEEE Trans. Power Electron.*, vol. 30, no. 8, pp. 4536–4547, Aug. 2015.
[42] F. Krismer and J. W. Kolar, "Efficiency-optimized high-current dual active bridge converter for automotive applications," *IEEE Trans. Ind. Electron.*, vol. 59, no. 7, pp. 2745–2760, Jul. 2012.
[43] S. Eren, M. Pahlevaninezhad, A. Bakhshai, and P. Jain, "An adaptive droop DC-bus voltage controller for a grid-connected voltage source inverter with LCL filter," *IEEE Trans. Power Electron.*, vol. 30, no. 2, pp. 547–560, Feb. 2014.
[44] *IEEE Adoption of Smart Energy Profile 2.0 Application Protocol Standard*, IEEE Std 2030.5-2013, Nov. 2013.
[45] N. C. F. Tse, W. H. Lau, and J. Y. C. Chan, "ZigBee based smart metering network for monitoring building integrated electric vehicle charging circuits," in *Proc. Power Energy Soc. General Meeting*, Jul. 2010, pp. 1–5.
[46] A. Tascikaraoglu, M. Uzunoglu, M. Tanrioven, A. R. Boynuegri, and O. Elma, "Smart grid-ready concept of a smart home prototype: A demonstration project in YTU," in *Proc. Power Eng., Energy Elect. Drives,* May 2013, pp. 1568–1573.
[47] R. Marino and P. Tomei, *Nonlinear Control Design: Geometric, Adaptive and Robust*. Englewood Cliffs, NJ, USA: Prentice Hall, Aug. 1995.
[48] A. Arsie and C. Ebenbauer, "Refining LaSalle's invariance principle," in *Proc. Amer. Control Conf.,* Jun. 2009, pp. 108–112.
[49] G. Chen, J. Zhou, and S. Celikovsky, "On LaSalle's invariance principle and its application to robust synchronization of general vector Lienard equations," *IEEE Trans. Autom. Control*, vol. 50, no. 6, pp. 869–874, Jun. 2005.
[50] J. P. Hespanha, "Uniform stability of switched linear systems: extensions of LaSalle's Invariance Principle," *IEEE Trans. Autom. Control*, vol. 49, no. 4, pp. 470–482, Apr. 2004.
[51] A. R. Teel, "Asymptotic convergence from Lp stability," *IEEE Trans. Autom. Control*, vol. 44, no. 11, pp. 2169–2170, Nov. 1999.
[52] S. Wiggins, *Introduction to Applied Nonlinear Dynamical Systems and Chaos*. New York, NY, USA: Springer, 2003.
[53] *CYCLONE IV Device Handbook*, Altera Corporation, San Jose, CA, USA, CYIV-53001-1.5, vol. 3, Nov. 2011.
[54] D. Bishop, "Fixed point package users guide," User Guide, Sep. 2005.
[55] E. Monmasson, L. Idkhajine, M. N. Cirstea, I. Bahri, A. Tisan, and M.-W. Naouar, "FPGAs in industrial control applications," *IEEE Trans. Ind. Informat.*, vol. 7, no. 2, pp. 224–243, May 2011.
[56] M.-W. Naouar, A. A. Naassani, E. Monmasson, and I. Slama-Belkhodja, "FPGA-based predictive current controller for synchronous machine speed drive," *IEEE Trans. Power Electron.*, vol. 23, no. 4, pp. 2115–2126, Jul. 2008.
[57] E. Monmasson, L. Idkhajine, and M. -W. Naouar, "FPGA-based controllers," *IEEE Ind. Electron. Mag.,*vol. 5, no. 1, pp. 14–26, Mar. 2011.
[58] E. Monmasson and M. N. Cirstea, "FPGA design methodology for industrial control systems: A review," *IEEE Trans. Ind. Electron.*, vol. 54, no. 4, pp. 1824–1842, Aug. 2007
[59] CEL MeshConnect, "Integrated transceiver modules for ZigBee/IEEE 802.15.4," Jul. 2014.
[60] P. Kokotovic, H. K. Khalil, and J. OReilly, *Singular Perturbation Methods in Control*. Philadelphia, PA, USA: SIAM, 1999.
[61] A. N. Tikhonov, "Systems of differential equations containing a small parameter multiplying the derivative," *Mat. Sb.*, vol. 31, pp. 575–586, 1952.
[62] F. Verhulst, *Methods and Applications of Singular Perturbations: Boundary Layers and Multiple Timescale Dynamics*. New York, NY, USA: Springer, 2005.
[63] W. Longke, W. J. Book, and J. D. Huggins, "Application of singular perturbation theory to hydraulic pump controlled systems," *IEEE Trans. Mechatron.*, vol. 17, no. 2, pp. 251–259, Apr. 2012.
[64] S. Celikovsky, S. Papacek, A. Cervantes-Herrera, and J. Ruiz-Leon, "Singular perturbation based solution to optimal microalgal growth problem and its innite time horizon analysis," *IEEE Trans. Autom. Control*, vol. 55, no. 3, pp. 767–772, Mar. 2010.
[65] P. Rodriguez, A. Luna, M. Ciobotaru, R. Teodorescu, and F. Blaabjerg, "Advanced grid synchronization system for power converters under unbalanced and distorted operating conditions," in *Proc. IEEE Ind. Electron.,* Nov. 2006, pp. 5173–5178.
[66] G. Fedele and A. Ferrise, "Non adaptive second-order generalized integrator for identification of a biased sinusoidal signal," *IEEE Trans. Autom. Control*, vol. 57, no. 7, pp. 1838–1842, Jul. 2012.
[67] P. Rodriguez, A. Luna, I. Candela, R. Teodorescu, and F. Blaabjerg, "Grid synchronization of power converters using multiple second order generalized integrators," in *Proc. Ind. Electron.,* Nov. 2008, pp. 755–760.
[68] M. Ciobotaru, R. Teodorescu, and F. Blaabjerg, "A new single-phase PLL structure based on second order generalized integrator," in *Proc. Power Electron. Spec. Conf.,* 2006, pp. 1–6.
[69] S. Golestan, M. Monfared, and F. D. Freijedo, "Design-oriented study of advanced synchronous reference frame phase-locked loops," *IEEE Trans. Power Electron.*, vol. 28, no. 2, pp. 765–778, Feb. 2013.
[70] M. M. Canteli, A. O. Fernandez, L. I. Eguiluz, and C. R. Estebanez, "Three-phase adaptive frequency measurement based on Clarke's transformation," *IEEE Trans. Power Del.*, vol. 21, no. 3, pp. 1101–1105, Jul. 2006.
[71] H. Liu, R. Ortega, and G. Damm, "A globally convergent frequency estimator," *IEEE Trans. Autom. Control*, vol. 44, no. 4, pp. 698–713, Apr. 1999.
[72] D. Yazdani, M. Pahlevaninezhad, and A. Bakhshai, "Three-phase grid synchronization techniques for grid connected converters in distributed generation systems," in *Proc. Ind. Electron. Int. Symp.*, Jul. 2009, pp. 1105–1110.
[73] M. Mascioli, M. Pahlevaninezhad, and P. Jain, "FPGA-based implementation of an adaptive notch filter used for grid synchronization of grid-connected converters," in *Proc. Ind. Electron. Soc.,* Nov. 2013, pp. 7617–7622.
[74] D. Yazdani, A. Bakhshai, G. Joos, and M. Mojiri, "A real-time selective harmonic extraction approach based on adaptive notch filtering," in *Proc. Ind. Electron. IEEE Int. Symp.*, 2008, pp. 226–230.
[75] M. Pahlevaninezhad, S. Eren, P. K. Jain, and A. Bakhshai, "Self-sustained oscillating control technique for current-driven full-bridge DC/DC converter," *IEEE Trans. Power Electron.*, vol. 28, no. 11, pp. 5293–5310, Nov. 2013.
[76] S. Eren, M. Pahlevaninezhad, A. Bakhshai, and P. K. Jain, "Composite nonlinear feedback control and stability analysis of a grid-connected voltage source inverter with LCL filter," *IEEE Trans. Ind. Electron.*, vol. 60, no. 11, pp. 5059–5074, Nov. 2013.
[77] Y. Kim, M. Kiemb, C. Park, J. Jung, and K. Choi, "Resource sharing and pipelining in coarse-grained reconfigurable architecture for domain-specific optimization," in *Proc. Design, Autom. Test Europe*, 2005, pp. 12–17.

Majid Pahlevani (S'07–M'12–SM'14) received the B.S and M.S degrees in electrical engineering from the Isfahan University of Technology, Isfahan, Iran, and the Ph.D. degree from Queens University, Kingston, ON, Canada.

He is currently a Research Associate with the Department of Electrical and Computer Engineering, Queens University, as well as a Senior Engineer in SPARQ Systems, Inc., Kingston. He worked as a Technical Designer in the Information and Communication Technology Institute, Isfahan University of Technology, from 2003 to 2007, where he was involved in design and implementation of high quality resonant converters. He also collaborated with Freescale Semiconductor Inc. where he was the leader of a research team working on the design and implementation of the power converters for a pure electric vehicle from 2008 to 2012. He is the author of more than 80 journal and conference proceeding papers and the holder of 16 U.S. patents (issued/pending). His current research interests include robust and nonlinear control in power electronics, advanced soft-switching methods in power converters, plug-in pure electric vehicles, and PV-microinverters.

Dr. Pahlevani is a Member of the IEEE Power Electronics Society and Industrial Electronics Society. He is also the recipient of the "Engineering and Applied Sciences Outstanding Thesis" award from Queens University, Canada, "Research Excellence Award" from IEEE Canada, and "Distinguished Graduate Student Award" from the Isfahan University of Technology.

Suzan Eren (S'07–M'13) received the B.Sc., M.Sc., and Ph.D. degrees in electrical engineering from Queens University, Kingston, ON, Canada, in 2006, 2008, and 2013, respectively.

She is currently a Postdoctoral Fellow at Queens University. She has published more than 20 journal and conference papers in the field of control and power electronics. She received the 2011–2012 Bert Wasmund Scholarship for Sustainable Energy Research. Her research interests include signal processing and control techniques for power converters, and her research particularly focuses on the control of grid-connected voltage source converters in renewable energy applications.

Josep M. Guerrero (S'01–M'04–SM'08–F'15) received the B.S. degree in telecommunications engineering, the M.S. degree in electronics engineering, and the Ph.D. degree in power electronics from the Technical University of Catalonia, Barcelona, Spain, in 1997, 2000, and 2003, respectively.

Since 2011, he has been a Full Professor with the Department of Energy Technology, Aalborg University, Aalborg, Denmark, where he is responsible for the Microgrid Research Program. From 2012, he is a Guest Professor at the Chinese Academy of Science and the Nanjing University of Aeronautics and Astronautics; from 2014, he is Chair Professor at Shandong University; and from 2015 he is a Distinguished Guest Professor at Hunan University. His research interests is oriented to different microgrid aspects, including power electronics, distributed energy-storage systems, hierarchical and cooperative control, energy management systems, and optimization of microgrids and islanded minigrids.

Dr. Guerrero is an Associate Editor for the IEEE TRANSACTIONS ON POWER ELECTRONICS, the IEEE TRANSACTIONS ON INDUSTRIAL ELECTRONICS, and the IEEE INDUSTRIAL ELECTRONICS MAGAZINE, and an Editor for the IEEE TRANSACTIONS ON SMART GRID and the IEEE TRANSACTIONS ON ENERGY CONVERSION. He has been Guest Editor of the IEEE TRANSACTIONS ON POWER ELECTRONICS SPECIAL ISSUES: POWER ELECTRONICS FOR WIND ENERGY CONVERSION AND POWER ELECTRONICS FOR MICROGRIDS; the IEEE TRANSACTIONS ON INDUSTRIAL ELECTRONICS SPECIAL SECTIONS: UNINTERRUPTIBLE POWER SUPPLIES SYSTEMS, RENEWABLE ENERGY SYSTEMS, DISTRIBUTED GENERATION AND MICROGRIDS, AND INDUSTRIAL APPLICATIONS AND IMPLEMENTATION ISSUES OF THE KALMAN FILTER; and the IEEE TRANSACTIONS ON SMART GRID SPECIAL ISSUE ON SMART DC DISTRIBUTION SYSTEMS. He was the Chair of the Renewable Energy Systems Technical Committee of the IEEE Industrial Electronics Society. In 2014, he was awarded by Thomson Reuters as Highly Cited Researcher, and in 2015, he was elevated as IEEE Fellow for his contributions on "distributed power systems and microgrids."

Praveen Jain (S'86–M'88–SM'91–F'02) received the B.E. degree (with honors) in electrical engineering from the University of Allahabad, Allahabad, India, in 1980, and the M.A.Sc. and Ph.D. degrees in electrical engineering from the University of Toronto, Toronto, ON, Canada, in 1984 and 1987, respectively.

He is a Founder of CHiL Semiconductor, Tewksbury, MA, USA, and SPARQ System, Kingston, ON. He was a Production Engineer with Crompton Greaves, a Design Engineer with ABB, a Senior Space Power Electronics Engineer with Canadian Astronautics Ltd., a Technical Advisor with Nortel, and a Professor with Concordia University, Montreal, QC, Canada. In addition, he has been a Consultant with Astec, Ballard Power, Freescale Semiconductors, Inc., General Electric, Intel, and Nortel. He is currently a Professor and a Canada Research Chair with the Department of Electrical and Computer Engineering, Queens University, Kingston, where he is also the Director of the Queens Centre for Energy and Power Electronics Research. He has supervised more than 75 graduate students, postdoctoral fellows, and research engineers. He has published more than 350 technical papers (including more than 90 IEEE transactions papers). He is the holder of more than 50 patents (granted and pending).

Dr. Jain is an Editor of the *International Journal of Power Electronics*. He is a Fellow of the Engineering Institute of Canada and the Canadian Academy of Engineering. He was the recipient of the 2004 Engineering Medal (R&D) from the Professional Engineers of Ontario and the 2011 IEEE William Newell Power Electronics Field Award. He is an Associate Editor of the IEEE TRANSACTIONS ON POWER ELECTRONICS. He is also a Distinguished Lecturer of the IEEE Industry Applications Society.